



## Review

## A critical review on temperature dependent irradiation response of high entropy alloys

Abid Hussain <sup>a</sup>, R.S. Dhaka <sup>b</sup>, Ho Jin Ryu <sup>c</sup>, Saurabh Kumar Sharma <sup>d</sup>, Pawan Kumar Kulriya <sup>d,\*</sup><sup>a</sup> Materials Science Group, Inter-University Accelerator Center, New-Delhi 110067, India<sup>b</sup> Department of Physics, Indian Institute of Technology Delhi, Hauz Khas, New-Delhi 110016, India<sup>c</sup> Department of Nuclear and Quantum Engineering, Korea Advanced Institute of Science and Technology (KAIST), Daejeon 305-701, the Republic of Korea<sup>d</sup> School of Physical Sciences, Jawaharlal Nehru University, New-Delhi 110067, India

## ARTICLE INFO

## Article history:

Received 7 December 2022

Received in revised form 18 February 2023

Accepted 8 March 2023

Available online 13 March 2023

## Keywords:

High entropy alloys

Phase stability

Lattice distortion

Irradiation effects

High temperature irradiation effects

## ABSTRACT

This article reviews the recent development in the understanding of the design parameters as well as mechanical properties and the radiation stability-based classification of the single-phase high entropy alloys (HEAs). Because of their excellent radiation tolerance, HEAs are proposed as the potential candidate for their application as a structural material in generation-IV nuclear reactors, where harsh environmental condition prevails. Theoretical calculation and experimental studies suggest that phase-stability and elemental distribution in the solid solution depend on the binary enthalpy of mixing, atomic size, electronegativity and magnetic nature of the elements. Energetic heavy ion irradiation investigations on the HEAs confirmed that the composition, chemical nature, number and size of alloying elements play an important role to determine their response to irradiation. Furthermore, irradiation stability at elevated temperatures also depends upon the incorporation of elements like Pd and Al in the solid solution. Phase stability, radiation-induced segregation (RIS) and bubble formation in HEAs are affected by both the irradiation temperature as well as the types of alloys and their microstructure. Finally, the improvement in structural stability in a high-temperature radiation environment and their applicability as structural materials in the nuclear reactor system have been reviewed.

© 2023 Elsevier B.V. All rights reserved.

## Contents

1. Introduction . . . . .	2
1.1. Empirical parameters to determine the phase of HEAs . . . . .	3
2. Types of HEAs . . . . .	3
3. Response to energetic ion irradiation . . . . .	4
3.1. Defects produced by energetic ions irradiation in HEAs . . . . .	4
3.2. Chemical complexity . . . . .	5
3.2.1. Intrinsic nature of alloying elements . . . . .	5
3.2.2. Concentration of the alloying elements . . . . .	5
3.2.3. Number of alloying elements . . . . .	6
3.3. Lattice distortion . . . . .	6
3.4. Microstructure . . . . .	7
4. High-temperature irradiation . . . . .	7
4.1. Irradiation-induced swelling . . . . .	7
4.2. Phase stability . . . . .	9
4.2.1. Radiation-induced segregation . . . . .	9

\* Corresponding author.

E-mail address: [pkkulriya@mail.jnu.ac.in](mailto:pkkulriya@mail.jnu.ac.in) (P.K. Kulriya).<sup>1</sup> 0000-0001-5563-7584

4.3. Bubble formation.....	11
5. Conclusions.....	12
6. Future scope.....	12
CRediT authorship contribution statement .....	13
Declaration of Competing Interest.....	13
Acknowledgement.....	13
References.....	13

## 1. Introduction

High entropy alloys (HEAs) are at the forefront of exploration in modern alloy systems. HEAs, reported by Yeh *et al.* [1] in 1995, are different from the traditional alloys because they contain at least 5 different elements in equiatomic ratios or nearly equiatomic ratios (in general 5–35 at%). These multi-component alloys exhibit superior physical properties like radiation resistance, high thermal and corrosion resistance, etc [2,3], which makes them a potential candidate for next-generation advanced nuclear fission and fusion systems [4]. The proposed operating temperature range for the next-generation reactor materials is (300–900)°C [5]. In this temperature range, the materials being used in various components of the reactors are austenitic stainless steel (type 304, 304 L), V and W alloys. Because of the presence of harsh radiation and chemical environment, these materials suffer from various failures like radiation-induced segregation, void swelling, irradiation creep, an-isotropic growth, inert gas bubble formation, [6,7] phase-segregation, etc. [8]. While HEAs, exhibit excellent properties such as high phase stability, thermal stability, oxidation resistance and mechanical and radiation stability [9,10] thus these HEAs are believed to be a suitable candidate for future reactor materials operating in extreme conditions of severe radiation damage at elevated temperatures. The origin of these intriguing properties of HEAs is believed to be from the presence of chemical short-range ordering (CSRO) which desirably changes the electronic structure, lattice dynamics, defects migration/recombination and thermodynamics in tune with the excellent properties. However, the experimental determination of CSRO was difficult because of its sub-nanometer changes in chemical ordering. Experimentally concrete evidence of the presence of CSRO was reported for the first time in NiCoV medium entropy alloy (MEA) by using an appropriate zone axis with elemental mapping TEM investigations [11]. Also from their studies the preferential bonding between unlike atoms (Ni-V, Co-V) as well as avoidance of similar V-V bonding in the first nearest neighbour was also observed in NiCoV MEA. A similar short-range ordering (SRO) was also observed in NiCoCr MEA in which unlike Ni-Cr, Cr-Co bonding favours while Cr-Cr bonding shows avoidance [12]. Several other medium/high entropy alloys unequivocally show experimental evidence of the presence of CSRO/SRO [13–15]. Further, it is speculated that the presence of SRO/CSRO will enhance the mechanical performance of the alloy by interaction with the moving dislocations [16]. Profuse dislocations tangling with CSRO/SRO region rather than a planner slip was observed and the slowdown of dislocation migration is thus expected thereby increasing the dislocation density [11,17]. Thus the SRO/CSRO can be used to tune the dislocation density and ultimately the hardening behaviour. R. Zhang *et al.* used the different thermal treatments after homogenization in NiCoCr MEA to tune the SRO/CSRO and its effect on the mechanical hardening [18], likewise the presence of CSRO/SRO also suppress the defects dynamics in HEAs thereby increasing the radiation stability [19].

The stability of HEAs at elevated temperatures is attributed to the higher entropy of mixing that minimizes Gibb's free energy [20]. Gibb's free energy is given by the equation.

$$\Delta G_{mix} = \Delta H_{mix} - T\Delta S_{mix} \quad (1)$$

Where  $\Delta G_{mix}$  and  $\Delta H_{mix}$  are Gibbs free energy and enthalpy of mixing, respectively. The configuration entropy is defined by the equation:

$$\Delta S_{mix} = -R \sum_{i=1}^N x_i \ln x_i \quad (2)$$

where  $x_i^s$  are the atomic fraction of  $i^{th}$  element and R is the gas constant. For example, equiatomic HEAs having 5 elements, the value of  $\Delta S_{mix}$  becomes  $1.6R \text{ Jmol}^{-1}\text{K}^{-1}$ . The value of configurational entropy is given by equation (2) for an ordered intermetallic phase gives ( $\Delta S_{mix} \approx 0$ ). In comparison, HEAs have a high value of  $\Delta S_{mix}$  because of mixing a large number of elements thus lowering the values of Gibb's free energy further, which helps in the formation of a more stable solid solution phase. The stability becomes even more pronounced at higher temperature because the  $T \Delta S_{mix}$  contribution to  $\Delta G_{mix}$  increases. Phase stability at high temperature is also important as one of the reasons for component failure at an elevated temperature is the phase transformation or secondary phase formation which activate corrosion or cracking. It must be noted that alloy micro-structure should also be stable at high temperatures because it may cause failure of the component by the phase transformation. Irradiation of crystalline materials by energetic ions can produce displacement in the atoms leading to various changes in the lattice ranging from point defects formation to crystalline-amorphous phase transition. Creation of such defects produces changes in the micro-structure and ultimately degrades the mechanical and physical properties of the materials. Irradiation experiment performed on nuclear ceramics e.g.  $\text{Gd}_2\text{Zr}_2\text{O}_7$  and doped  $\text{Gd}_2\text{-Zr}_2\text{O}_7$  [21–24], pure metals (e.g. tungsten) [25] and various HEAs [26–28] show modifications in the micro-structure on energetic ion irradiation. Advanced characterization techniques like glancing incident X-ray diffraction (GIXRD), scanning electron microscopy (SEM), and transmission electron microscopy (TEM) are being used to characterize various structural and micro-structural changes in these materials due to ion irradiation.

This paper thus summarises the various aspect of HEAs for their applicability as a structural material for advanced nuclear reactor systems. Several HEAs have been identified for this purpose. For example, void swelling resistance of NiCoCrFePd after replacing Mn with Pd in NiCoCrFeMn alloy was enhanced when irradiated with 3 MeV  $\text{Ni}^{2+}$  up to a fluence  $5 \times 10^{16} \text{ ions/cm}^2$  at 853 K as reported by Lu *et al.* [29]. NiCoCrFePd HEAs showed excellent phase stability with no phase transformation till 74.0 GPa, whereas NiCoCr and NiCoCrFe alloys exhibit fcc to hcp phase transformations at a pressure of 45 GPa and 13.5 GPa [30]. A few reports suggest that mechanical, chemical and radiation tolerance of NiCoCrFe HEAs can be improved by the addition of aluminium (Al) [31–33]. Microstructural analysis of NiCoCrFeCu HEA confirmed the formation of the matrix phase and Cu-rich phase on the incorporation of Cu. This Cu-rich phase showed a pronounced swelling than the matrix phase when NiCoCrFeCu HEA is irradiated with 100 keV  $\text{He}^+$  beam at a fluence of  $5 \times 10^{17} \text{ ions/cm}^2$ . The above reports suggest that HEAs stability is critically dependent upon the structure of the alloys. Based on the structure, HEAs studied to date have shown single-phase body-centered cubic (bcc), face-centered cubic (fcc), and hexagonal close-packed (hcp) crystal structures. It is reported that different

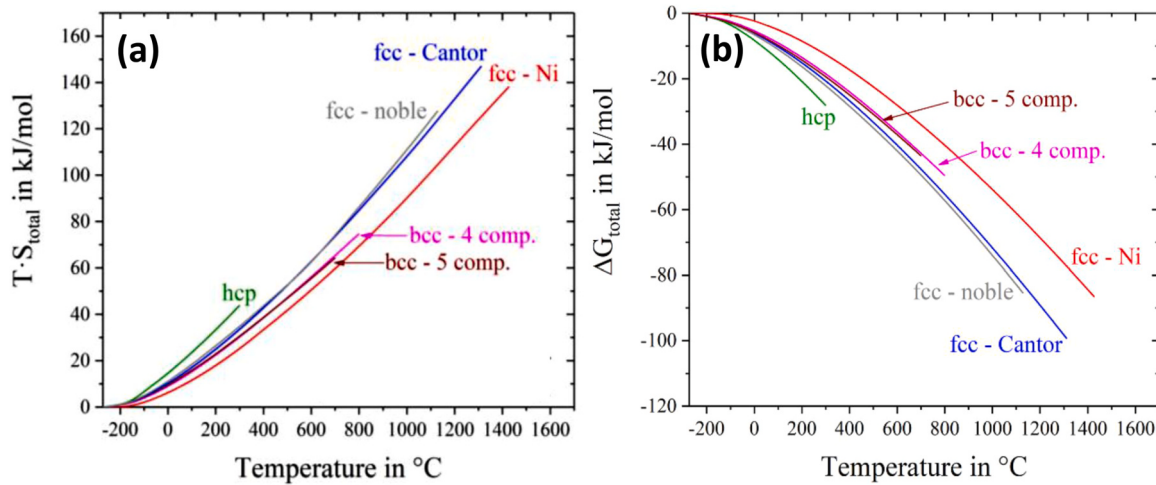


**Figure 1.** Temperature-dependent (a)  $TS_{total}$  for fcc Ni and various high entropy alloys and (b) contribution of entropy to Gibbs's free energy [34]. (Figure adapted from [34] under licence: <https://creativecommons.org/licenses/by/4.0/>).

structures have different entropy products  $TS_{total}$  where  $S_{total}$  is the sum of thermal entropy and configurational entropy. It is observed that the hcp structure has the highest value of  $S_{total}$  and the bcc structure has the least value [34]. This suggests that only a similar structure can be used to investigate the effect of entropy on the stability of the solid solution. The product of total entropy and temperature gives a contribution to the Gibbs free energy as shown in Fig. 1 using the equation:

$$\Delta G_{total} = \Delta H - T\Delta S_{total} \quad (3)$$

With

$$\begin{aligned} \Delta H &= \int_0^T C_p dt \text{ and } \Delta S_{total} = S_{conf.} + \int_0^T C_p \frac{1}{T} dt \\ \Delta G_{total} &= \int_0^T C_p dt - T \left( \Delta S_{conf.} + \int_0^T C_p \frac{1}{T} dt \right) \end{aligned} \quad (4)$$

where  $C_p$  is the heat capacity at constant pressure and  $S_{conf.}$  is the configurational entropy. Haas *et al.* [34] reported that configurational entropy plays a key role in the stabilization of solid solutions in the case of fcc Ni and fcc Cantor. This suggests that the new alloys combination resulting from the replacement of a single element of well known single-phase Cantor alloy should be a single-phase solid solution but contrary results are reported by Otto *et al.* [35]. Thus, the configurational entropy is not the only factor which determines the stability of alloy but several other factors like mixing enthalpy ( $\Delta H_{mix}$ ) [35–37] and atomic size difference ( $\delta$ ) are also important for stabilizing the solid solution [38]. Thus, the strategy of maximizing only the configurational entropy to get single-phase solid solution may not be useful. Furthermore, annealing temperature also plays a key role in the phase stability of the HEAs. It has been reported that the single-phase HEA can be solidified into the inter-metalllic phases on annealing [39–43]. Thus, phase instability and the formation of secondary phases need special attention for their applications in high-temperature environments like in the next-generation nuclear reactors.

### 1.1. Empirical parameters to determine the phase of HEAs

The formation of a solid solution is decided by two unitless quantities namely  $\delta$  and  $\Omega$  defined as:

$$\delta = \sqrt{\sum_{i=1}^n x_i \left(1 - \frac{r_i}{\bar{r}}\right)^2} \times 100 \quad (5)$$

$$\Omega = T_m \frac{\Delta S_{mix}}{|\Delta H_{mix}|} \quad (6)$$

$$\Delta H_{mix} = \sum_{i \neq j=1}^n x_i x_j \Delta H_{ij} \quad (7)$$

Where  $x_i$ ,  $n$ ,  $r_i$ ,  $\bar{r}$ ,  $T_m$ ,  $\Delta S_{mix}$ ,  $\Delta H_{ij}$  and  $\Delta H_{mix}$  are atomic fraction, the number of elements, the radius of  $i^{th}$  atom, average radius, melting temperature, the entropy of mixing, and enthalpy of mixing respectively. Yang *et al.* [44] predicted that a solid solution can be formed if the values of  $\delta \leq 6.6$  and  $\Omega \geq 1.1$ , otherwise intermetallic or a bulk metallic glass is formed. The control over the phase in a solid solution is decided by the thermodynamic parameters  $\Delta G_{mix}$  and  $T_m \Delta S_{mix}$ , if the kinetic factor is not included. As stated in the Gibbs free energy equation (1), the thermodynamic phase is determined by the competition between  $\Delta G_{mix}$  and  $T_m \Delta S_{mix}$ . The range of empirical parameters calculated using equations (5) and (7) for the formation of single-phase, multi-phase and amorphous are given below:

1.  $-15 \text{ kJ/mol} \leq \Delta H_{mix} \leq 5 \text{ kJ/mol}$  and  $0 < \delta \leq 6.6$  (Single Phase)
2.  $-20 \text{ kJ/mol} \leq \Delta H_{mix} \leq -15 \text{ kJ/mol}$  and  $6.6 < \delta \leq 9$  (Multiphase)
3.  $-49 \text{ kJ/mol} \leq \Delta H_{mix} \leq -25 \text{ kJ/mol}$  and  $\delta \geq 9$  (Amorphous)

In the case of a single-phase solid solution, the crystal structure of the alloys can be estimated using the value of valance electron concentration (VEC), defined as  $\sum_{i=1}^n x_i (\text{VEC})_i$ , Where 'n' is the number of element and  $x_i$ s are the atomic fractions. The values of the VECs are given as [45]: .

1.  $\text{VEC} \geq 8.0 \Rightarrow (\text{FCC})$
2.  $\text{VEC} = 6.8-8.0 \Rightarrow (\text{FCC+BCC})$
3.  $\text{VEC} < 6.8 \Rightarrow (\text{BCC})$

### 2. Types of HEAs

As discussed above, on the basis of different physical properties, it is hard to see a clear trend in the HEAs. However, Diao *et al.* [46] classified HEAs into four groups based on their mechanical properties.

- (a) Type-I: Soft HEAs solid solution which includes 3d-transition metals.
- (b) Type-II: Combination of transition metals with P block large atomic radii.
- (c) Type-III: Refractory metal alloys.

**Table 1**

Classification of HEAs based upon temperature dependent yield strength (Reprinted under licence: <https://creativecommons.org/licenses/by/4.0/>).

Type-I (Transition metals soft HEAs)	Type-II (P-block element incorporated HEAs)	Types-III (Refractory HEAs)	Type-IV (Large transitional metal incorporated HEAs)
NiCoCrFeMn	Al <sub>x</sub> NiCoCrFe	HfNbTaTiZr	NiFeCoPd
NiCoCrFe	Al <sub>x</sub> NiCoCrFeMn	HfNbTaVZr	NiCrCoFePd
NiCoCrMn	Al <sub>x</sub> NiCoCuCrFe	HfNbTiZr	DyGdLuTbTm
NiFeCrMn	AlNiCoCuCrFeTi <sub>x</sub>	MoNbTaVZr	CoFeReRu
NiCoCuCrFe	NiCoCuCrFeV <sub>x</sub>	MoNbTaTiV	MoPdRhRu
NiCoCuMnFe	AlNiCoCrFe	NbTaTiV	Al <sub>x</sub> NiCoCrFeV

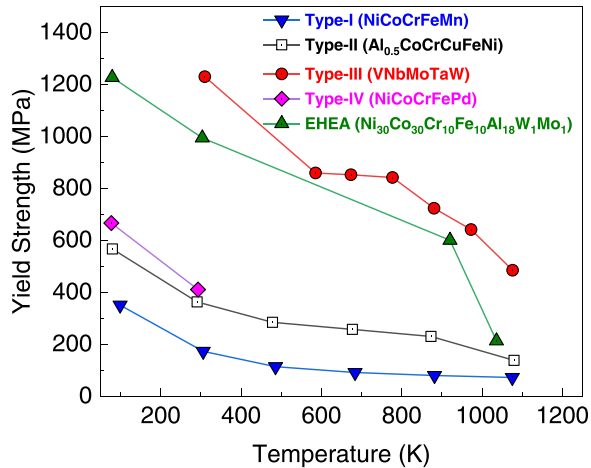


**Figure 2.** Variation of the yield strength with temperature for type-I, type-II, type-III, type-IV alloys. Calculated using data from Refs. [9,52–55].

(d) Type IV: Large transitional metals incorporated alloys.

**Table 1** lists the classification of different types of HEAs based on the yield strength. The yield strengths of different types of alloys critically depend upon the temperature of the material as shown in **Fig. 2**. It can be clearly seen that the yield strength of type-I alloys is lower than that of type-II and type-III. The high yield strength in the case of type-II and type-III is attributed to the addition of atoms with a large atomic radius like Al, Ti, V, and Mo in 3d transition elements. It may be noted that the yield strength of type-I and type-II abruptly decreases at high temperatures. However, the yield strength of type-III alloys at very high temperatures (~1000 K) is about 5 times higher than that of the type-II and also remains fairly constant even if the temperature is further increased to 2000 K. But the ductility of such alloys were found limited compared to the type-I alloys. Thus, a new type of alloy namely AlCoCrFeNi<sub>2.1</sub> eutectic high entropy alloys (EHEA) was designed first by Yiping Lu *et al.* which has the combination of both strength as well as ductility [47]. Many more new EHEA developed recently for example AlCrFeNiMo<sub>0.2</sub> [48], Co<sub>2</sub>Mo<sub>0.8</sub>Ni<sub>2</sub>VW<sub>0.8</sub> [49], FeCoNi<sub>2</sub>Al<sub>0.9</sub> [50] and Al<sub>5</sub>(CoNiV)<sub>95</sub> [51]. After an initial inspection of the eutectic phase, the presence of mostly dual phase with FCC and B<sub>2</sub> or FCC and Laves phases was found responsible for such a tunable strength as well as ductility over a wide range of temperature. The yield strengths of AlCr<sub>1.3</sub>TiNi<sub>2</sub>, and Ni<sub>30</sub>Co<sub>30</sub>Cr<sub>10</sub>Fe<sub>10</sub>Al<sub>18</sub>W<sub>1</sub>Mo<sub>1</sub> EHEA were found higher than type-I but comparable to type-II over a wide range of high temperature as shown in **Fig. 2**. This clearly suggests that such types of alloys are suitable for high-temperature environments.

### 3. Response to energetic ion irradiation

It is well established that the interaction of low-energy ions with solid matter leads to the creation of Primary Knock-on Atoms (PKAs). These PKAs migrate from their original position and distribute their

energy to surrounding atoms that produce additional knock-on atoms. The damage event occurs in a 10<sup>-11</sup> sec (10 ps) time frame generating a cascade of point defects and finally leaves PKAs as an interstitial atoms. Quantification of such defects is done by the value of displacement per atom (dpa) which is defined as

$$dpa = \frac{N_{\text{displacement}} \times \text{fluence}}{\text{Atomic density}} \quad (8)$$

As given in equation (8), dpa depends upon the number of displacements produced by the irradiating particles, the ion fluence which is the number of particles irradiated per unit area and the atomic density of the material. It is worth mentioning here that damage produced by the energetic particle also depends upon the nature of the particle and thus different for neutron, electron and heavy ions. The penetration depth (range) of the electrically neutral neutrons is about a few millimeters whereas heavy ions lose their energy quickly and can penetrate between 0.1 to 100  $\mu\text{m}$  only. In addition, the mass of the particle is also important because light particle (electrons and protons) produce damage limited to Frenkel pairs or small clusters whereas heavy ions and neutrons produce damage in the large clusters. In the case of HEAs, high dpa is required to observe the significant damage produced by using the neutron which takes prolonged exposure time as well as a very high neutron flux to simulate a reactor environment. Therefore, researchers are using a surrogate approach in which materials are exposed to the energetic heavy ions at particle accelerators to simulate the damage produced by the neutrons. Due to very high energy dumped by the energetic ions, one can produce very high dpa within a few hours.

#### 3.1. Defects produced by energetic ions irradiation in HEAs

Various reports related to low energy ion irradiation studies on HEAs suggest that several degradation phenomena like inert gas bubble formation, void swelling, amorphization, radiation-induced stress, corrosion, cracking, and radiation-induced segregation (RIS) happen in the alloy [56]. Among these, void swelling, inert gas bubbles formation [57,58] and radiation-induced segregation are extremely important challenges for the design of advanced radiation-resistant alloys with an extended performance in extreme conditions. The void swelling and inert gas bubbles can cause an unacceptable dimensional change in the material which causes the degradation of material causing fractures and reducing the toughness [8,59]. Several reports on conventional NiFeCr single-phase alloys suggest that the formation of the voids starts for an irradiation dose of > 1 dpa and at a temperature around 500°C at which the vacancies become mobile [60]. On exposure to higher temperatures (500–700)°C, swelling in the alloys is observed due to the accumulation of voids at elevated temperatures. Such phenomenal changes ultimately have a significant impact on the active lifetime of the structural materials employed in the reactor due to mechanical failure of the structural components [61,62].

Other phenomena like radiation-induced segregation (RIS) in which the local composition of the alloy gets altered by the coupled motion of solute with the vacancy or interstitial-type point defects

are also observed in the conventional alloys (NiCrFe and NiCrMn) on radiation with (0.1–1) dpa at 250°C temperature [63]. The mechanism of controlling RIS in steels is more generally associated with inverse Kirkendall (vacancy effects) in which the solute drag is coupled with the diffusion flow of vacancies or interstitials [62,64,65]. This coupled motion results in the enrichment of Ni and depletion of Cr and Mn solute elements at the point defect sinks such as grain boundaries which lead to phase instability, embitterment, stress and production of corrosion and cracking in the alloy [61,62]. In comparison to conventional alloys, HEAs exhibit a reduction in void swelling, suppression of RIS and Helium gas bubble accumulation [66–68]. For example, Yang *et al.* did not observe any void in NiCoCrFeMn and NiCoCrFePd HEAs after irradiation with  $\text{Ni}^{+2}$  ion to a fluence  $5 \times 10^{16}$  ions/cm $^2$  [69]. This extraordinary behaviour of HEAs is attributed to their complex composition and trapping of vacancies which favours the annihilation with interstitial because of high local lattice stress and high distortion in the lattice [26]. Due to these prevailing phenomena, the defects (including vacancies, dislocation and interstitial) created by the energetic ion become immobile which leads to a reduction in the voids and large dislocation structures in the HEAs. The following are key factors that affect the overall radiation-resistant response of HEAs:

- A. Chemical complexity
- B. Lattice distortion
- C. Micro-structure

### 3.2. Chemical complexity

The chemical complexity of alloy plays an important role in determining the radiation tolerance of the HEAs. It has been observed that the production of defects such as dislocation loops, precipitates and secondary phase formation can be seized by tuning the complexity of the alloys. It can be easily done by altering the concentration of the alloying elements, their type and the number of elements present in the alloys.

#### 3.2.1. Intrinsic nature of alloying elements

The structure of the alloys critically depends upon the elements present in the alloy. The radiation damage studies on the Ni-based fcc multi-component alloys showed that the response to radiation damage depends upon the size and chemical nature of the elements. The Rutherford backscattering spectrometry (RBS) technique is used to investigate the radiation damage in the Fe and Cr doped NiCo

alloy. Fig. 3 shows the RBS spectrum of (a) Ni, NiCoFe and NiCoCr alloys and (b) effect of Fe and Co in the Ni-based alloys. Change in the backscattering yield [Fig. 3(a)] with different doped elements signifies the effect of the type of elements. The backscattering yield in the case of pure Ni is higher than that of the NiCoCr and NiCoFe clearly showing that radiation damage is prominently affected by the type of element present in the alloy. Fig. 3(b) shows that a reduction in the irradiation-induced damage buildup is higher in NiFe alloys in comparison to NiCr alloys. The damage depth profile predicted from the stopping and range of ions in matter (SRIM) showed that the depth range of the defect clusters in Ni is more as compared to NiCo and NiFe, suggesting the mobility of defects in these disordered alloys is more restricted compared to pure element Ni [70].

Similarly, radiation-induced swelling in the Ni-based alloys is also reduced by alloying with manganese [27]. In the case of Ni-CoCrFePd alloys, Pd incorporation has a dramatic effect on the size of dislocation and density of the dislocation loops produced by ion irradiation. It has been reported that NiCoCrFePd has a higher density and smaller dislocation as compared to the NiCoCrFeMn alloy [29]. In the Pd-HEA, the average dislocation size is approximately four times smaller than Mn-HEA. Similarly, dislocation size in Mn-HEA was found two times smaller than NiCoCrFe alloy when irradiated with 3 MeV  $\text{Ni}^{+2}$  ions up to  $55 \pm 5$  dpa and  $38 \pm 5$  dpa, respectively [73]. Large local lattice distortion in Pd-HEA affects the growth of dislocation loops. The reported value of the local lattice distortion in the case of Pd-HEA is one order of magnitude higher than that in Mn-HEA [74]. Secondly, in the NiCoCr solid solution where Ni has a strong tendency to form a bond with Cr and Co as compared to Ni itself also helps in making a random solid solution [71]. Thus, it is important to note down here that the type of element present in an alloy plays a crucial role in making the alloy disordered. Therefore, the tendency to form a disordered solid solution with a strong lattice distortion due to the incorporation of large size elements is responsible for the enhancement of the radiation response in these multicomponent alloys. These results suggest that the intrinsic nature of elements affects the local environment which leads to improvement in the radiation tolerance of the HEAs.

#### 3.2.2. Concentration of the alloying elements

It has been reported that the various radiation-induced phenomena like swelling, radiation-induced segregation and bubble formation depend on the concentration of the alloying elements [66,75,76]. The importance of the concentration of the element is observed when the effect of Fe concentration on the radiation

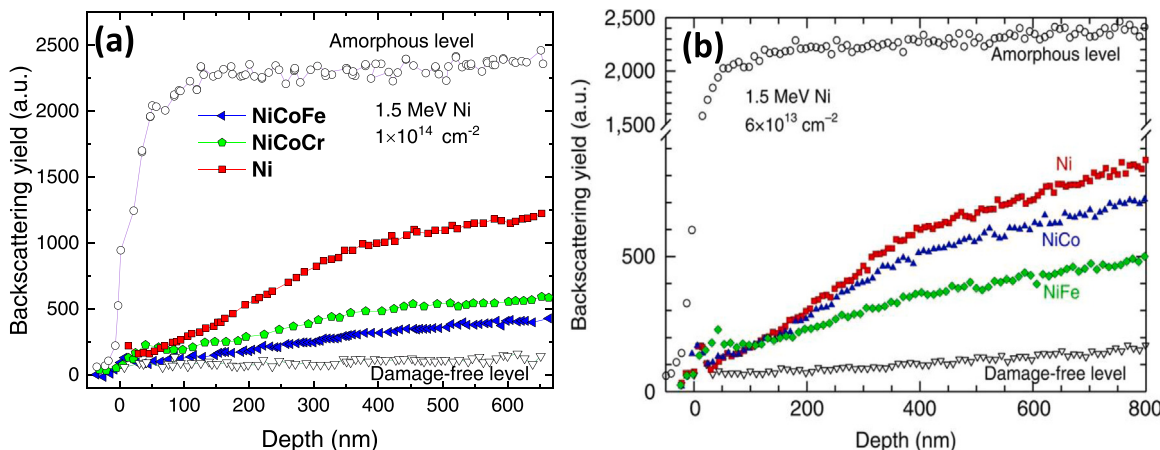


**Figure 3.** (a) The effect of Fe and Cr in NiCoCr and NiCoFe ternary equiatomic alloys on the irradiation response is shown by backscattering yield after irradiated with 1.5 MeV Ni ions to a fluence of  $1 \times 10^{14}$  ions/cm $^2$  (b) Effect of Fe and Co in NiFe and NiCo binary alloy on irradiation response shown by backscattering yield after irradiated with 1.5 MeV Ni ions to a fluence of  $6 \times 10^{13}$  ions/cm $^2$  [27,71,72].

Figure(b) adapted from Ref.[27] under licence:https://creativecommons.org/licenses/by/4.0/).

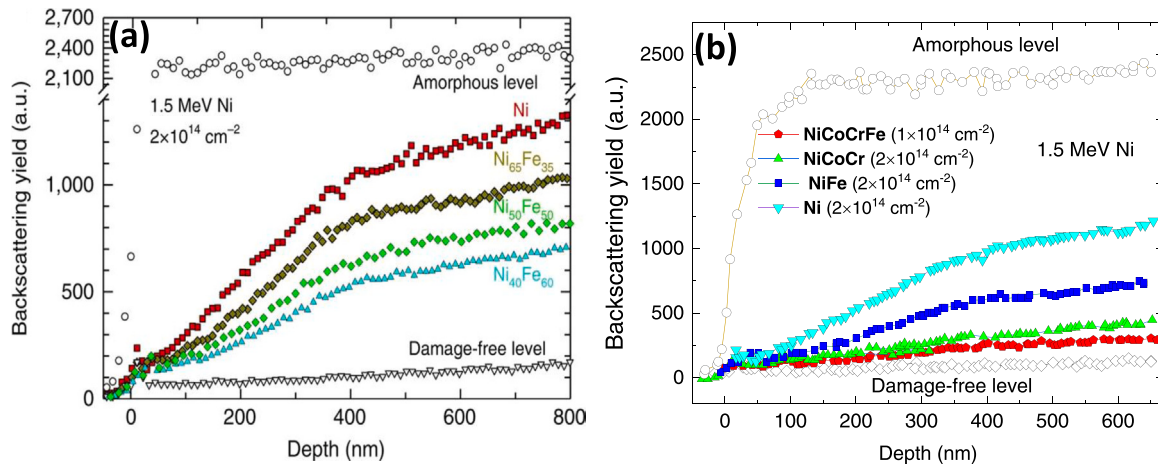


**Figure 4.** (a) RBS spectrum of pure Ni and Ni-Fe alloys irradiated with 1.5 MeV Ni ions to a fluence of  $2 \times 10^{14}$  ions/cm<sup>2</sup>. An increase in the backscattering yield with the increase in Fe concentration from 25 to 60 at% showing the pronounced effect of concentration on the radiation resistance response (b) Backscattering yield also increased with increasing the number of elements from Ni to NiCoCrFe irradiated with 1.5 MeV Ni ions to an ion fluence of  $1 \times 10^{14}$  ions/cm<sup>2</sup> and  $2 \times 10^{14}$  ions/cm<sup>2</sup> [27,71,72]. (Figure(a) adapted from Ref.[27] under licence:https://creativecommons.org/licenses/by/4.0/).

tolerance of the NiFe binary is investigated. Jin *et al.* irradiated NiFe single crystal with 1.5 MeV Ni ions to a fluence  $3 \times 10^{15}$  ions/cm<sup>2</sup> and investigated using Rutherford backscattering and channeling experiment (RBS/C). An enhancement in the radiation tolerance with an increase in Fe concentration (60 at%) is observed which is attributed to the slow down of interstitial aggregation with the increase in Fe concentration [66]. Fig. 4(a) shows the increase in the backscattering yield with the increase in Fe concentration from 35 at % to 60 at% in a binary NiFe alloy after irradiation with 1.5 MeV Ni ion to a fluence of  $2 \times 10^{14}$  ions/cm<sup>2</sup> [72]. A similar trend was also observed in the dislocation size analysed using the TEM [76]. It has been argued by using Extended X-Ray Absorption Fine Structure (EXAFS) measurement that local lattice distortion is enhanced by the increase in the separation between the nearest neighbour (Ni-Fe, Ni-Ni) on increasing Fe concentration in NiFe alloys [77]. Similarly, Zhang *et al.* [78] also systematically studied the effect of Pd concentration on the lattice distortion by using anomalous X-ray diffraction and X-ray absorption measurements in NiPd alloy. An increase in Ni-Pd bond length and coordination number for alloys having high Pd concentration (e.g. Ni<sub>50</sub>Pd<sub>50</sub> alloy) revealed the presence of distorted local structure in NiPd alloys. EXAFS studies also exhibited that Pd tends to bond with Pd in Ni<sub>20</sub>Pd<sub>80</sub> thereby promoting short-range ordering, while Ni tends to bond with Pd in Ni<sub>50</sub>Pd<sub>50</sub> forming a disordered solution. This suggests that the radiation response of the alloy can be controlled by changing the local chemical environment of the alloy system. The reduction in the number of the nearest neighbour is also higher in Ni<sub>20</sub>Pd than Ni<sub>50</sub>Pd on ion irradiation. Thus, the radiation damage tolerance of any material is specific to elemental and the local environments in the alloy which helps in controlling energy dissipation.

### 3.2.3. Number of alloying elements

Another important parameter that affects the radiation tolerance of a material is the number of alloying elements present in the alloy. The RBS/C studies carried out by Granberg *et al.* showed a major reduction in the damage upon irradiation with 1.5 MeV Ni<sup>+</sup> ion in the NiFe and NiCoCr as compared to Ni. It is argued that a significant reduction in the dislocation mobility with the increase in the number of elements leads to constrained movement of dislocations that forbids the formation of complex large defects [71]. Further, smaller size dislocation is also observed in NiFe alloy as compared to pure Ni element. On 3 MeV Ni<sup>+</sup> ion irradiation to a fluence  $5 \times 10^{16}$  ions/cm<sup>2</sup>, very small size dislocation is formed in the alloys having a large number of elements (e.g. NiCoCrFeMn and NiCoCrFePd) [79].

Thus the number of elements has an enormous effect on the defect dynamics. This effect is further investigated by the performance evaluation of binary (NiFe), ternary (NiCoCr) and more complex quaternary NiCoCrFe equiatomic alloys. The RBS/C investigations [Fig. 4(b)] performed on alloys irradiated with 1.5 MeV Ni ions to a fluence of  $1 \times 10^{14}$  ions/cm<sup>2</sup> and  $2 \times 10^{14}$  ions/cm<sup>2</sup> showed that the lowest backscattering yield is corresponding to NiCoFeCr followed by NiCoCr, NiFe and highest for pure Ni element. This suggests alloys having a large number of elements are more radiation stable. However, it is not always necessary that alloys containing more elements should have higher radiation stability. As shown in Fig. 3(a), irradiation response of both NiCoCr and NiCoFe is not the same. Because these two alloys show different backscattering yields under the same irradiation condition. Therefore, the radiation stability of the alloys is not only determined by the number of elements but also by the intrinsic nature of the elements present in the alloy.

Thus, the chemical complexity where the substitution of elements in the solid solution with another, change of composition of the elements and changing the number of alloying elements have a great impact on the energy dissipation processes and ultimately affects the formation and evolution of defects. Furthermore, the irradiation-induced interstitial, vacancies, dislocation loops and defect clusters are also affected by the chemical disorder and lattice distortion or lattice strain in the alloy.

### 3.3. Lattice distortion

Lattice distortion such as lattice strain and short-range ordering (SRO) in alloys is another parameter that significantly affects the structural stability of alloys against severe radiation dose which is studied by using the EXAFS technique, where the local lattice strain is defined as:

$$\epsilon_{ist} = \frac{a_{ist} - a_{ave}}{a_{ave}} \quad (9)$$

Where,  $a_{ist}$  is the lattice constant obtained from the fitting of the first peak in the pair distribution function (PDF), and  $a_{ave}$  is the lattice constant value obtained from the fitting of the entire spectrum in the PDF. Zhang *et al.* [78,80] reported the existence of concentration dependence of SRO in Ni<sub>80</sub>Pd<sub>20</sub> and Ni<sub>50</sub>Pd<sub>50</sub> binary alloys. They observed alternation in the SRO of the alloy because of the movement of atoms from the equilibrium positions [78]. In the case of equiatomic composition, highly distorted structure and SRO are observed due to the preferential bonding of Pd-Ni in comparison to

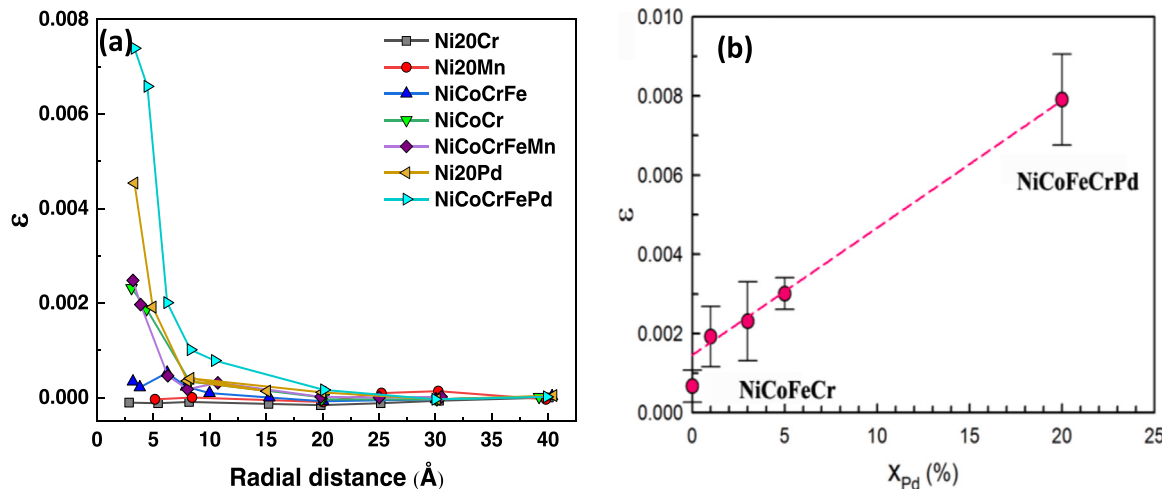


**Figure 5.** EXAFS spectrum for the evaluation of local lattice strain showing (a) the effect of different elements on the local lattice distortion in HEAs and (b) effect of different doping percentage of Pd atom on local lattice distortion in NiCoFeCr HEA [68,74,81,80]. (Figure(b) adapted from Ref. [81] under licence: <https://creativecommons.org/licenses/by/4.0/>).

Pd-Pd. At the low dose ( $\approx 0.1$  dpa), Ni-Pd and Pd-Pd bonds increase and then become constant. The number of Pd atoms in 1<sup>st</sup> coordination shell also decreases in both cases up to 0.1 dpa and then increases, signifying the effect of ion irradiation on SRO. The SRO is also found to be enhanced on ion irradiation up to 0.3 dpa.

Similar, EXAFS and neutron diffraction studies on local distortion in more complex medium entropy NiCoCr alloy reveal that Cr atoms have a higher tendency to bind with Ni and Co that prompts the enhancement in the SRO in the lattice as well as radiation resistance [71]. The EXAFS analysis of HEAs containing different series of Ni-CoCr, NiCoCrFe and NiCoCrFeMn HEAs shows that local lattice distortion increases with the increase in complexity. It is also noticed that alloys containing Pd show highly distorted lattice structure compared to others and the trend goes like NiCoCrFePd > Ni<sub>20</sub>Pd > NiCoCrFeMn = NiCoCr > NiCoCrFe > Ni<sub>20</sub>Mn Ni<sub>20</sub>Cr as shown in Fig. 5(a) [68]. Tong et al. [74] also compared the effect of Pd and Mn on the local lattice distortion in FeCoNiCr [Fig. 5(a)] and found that Pd creates appreciable short-range lattice strain in the lattice as compared to the Mn (1.35 Å). Such behaviour is attributed to the very large size of Pd ( $r = 1.38$  Å). Thus, the Pd atoms induce a strong lattice distortion which increases with the increase in Pd concentration [Fig. 5(b)]. Thus, the presence of large lattice distortion can cause the pinning of irradiation-induced dislocation or the defects which lead to enhancement of radiation resistance in Pd-containing HEAs [81]. To support this fact the electron microscopy investigations showed higher dislocation density and small size of dislocation in the Pd-containing alloys that again confirmed the higher radiation tolerance of Pd-containing alloys [29,82].

It is important to note down here that the effect of Pd on the lattice distortion in a quaternary system of alloys is more pronounced than in a binary system. Further, there is no change in the local lattice strain from the ternary system to the quaternary system suggesting that the number of elements is not the only factor responsible for the local lattice distortion but also the nature of the element is important.

### 3.4. Microstructure

The microstructure of the as-prepared alloys plays an important role in the energy dissipation process by energetic ions. Nano-crystalline and ultrafine grains show exceptional radiation damage tolerance as compared to coarse grain micro-structure because of the presence of a high density of grain boundaries, which acts as a defect sink [83]. Normally, annihilation of vacancies and interstitials take

place at these grain boundaries. Thus, grain boundary refinements are proposed as one of the ways to enhance radiation damage tolerance. The grain size, hence the micro-structure is generally controlled by annealing temperature and concentration of the elements present in the alloys. Recently Barr *et al.* [84] reported the effect of 2.8 MeV Au<sup>4+</sup> ion irradiation on nano-crystalline platinum (Pt) thin films having different grain sizes. The in-situ TEM studies on Pt thin films showed a larger dislocation loop size in the bigger grain size sample. This is attributed to the coalescence of small defects in the centre of large grain which effectively reduces the density thus increasing the radiation damage probability in large grain size. Shaofei *et al.* modified the micro-structure of NiCoCr by the incorporation of Si. The average grain size decreased from 6.8 μm for NiCoCr to 3.4 μm on the addition of 3.40 at% of Si and to 1.6 μm for addition of 6.18 at% Si [85]. On 0.275 MeV He ion irradiation at a fluence of  $5.14 \times 10^{16}$  ions/cm<sup>2</sup> and at a 600°C temperature, the average bubble size in 3.40 at% of Si(NiCoCr) was 12.3% smaller than in NiCoCr alloys. This clearly demonstrates the effect of microstructure on the irradiation-induced bubble formation in multi-component alloys.

## 4. High-temperature irradiation

In addition to the above discussed parameters, there are a few other experimental parameters such as the energy of ions, ion fluence, flux and temperature of the target materials that are used to simulate the performance of the alloys. Among these, the temperature of the target is very crucial because defects produced by the energetic ions may be annihilated or more complex structures can be formed because of the thermally assisted diffusion of vacancies leading to the formation of voids, swelling, and bubble formations. In general, structures like dislocation loops, precipitates, and secondary phase formation are observed at high temperatures due to the thermally activated movement of vacancies. The following subsection will focus on the dominating structural changes observed in alloy systems irradiated at elevated temperatures.

### 4.1. Irradiation-induced swelling

It is well established that a large number of defect clusters are produced during low-energy irradiation [86]. At a temperature of about  $(0.3\text{--}0.6)T_m$ , where  $T_m$  is the melting temperature, the defect clusters move along the burger vectors towards a distant position or a sink, leaving behind a highly vacant position and thus leading to the accumulation of void which is called swelling. Due to swelling,

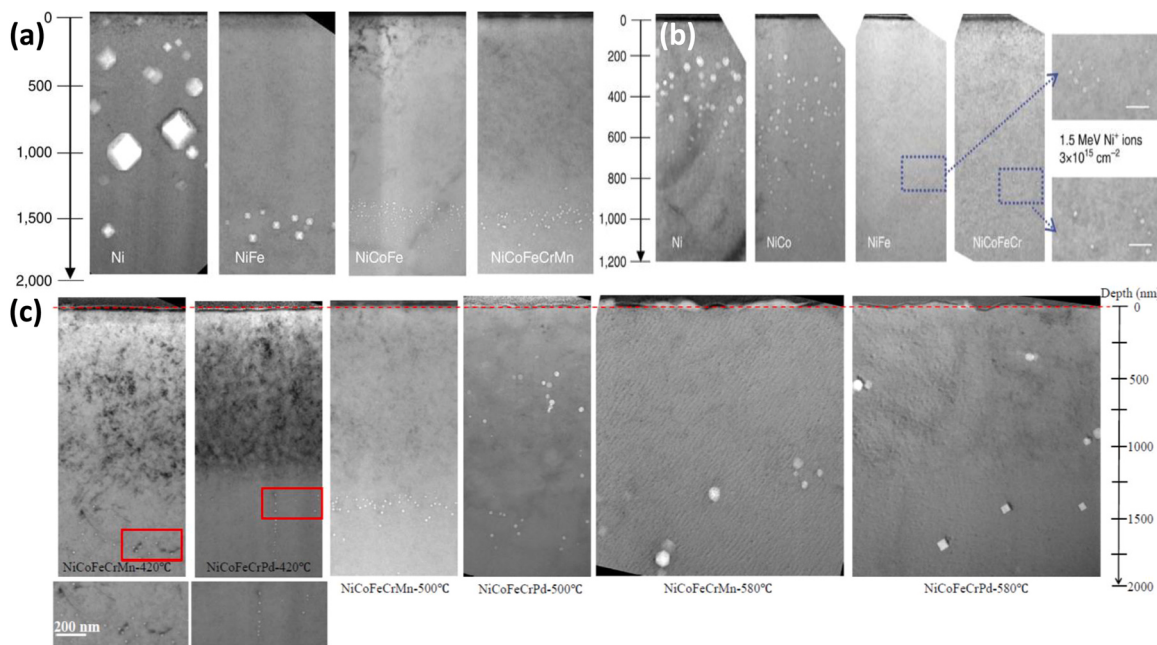


**Figure 6.** (a) Cross-sectional TEM image of 3.0 MeV irradiated Ni, NiFe, NiCoFe, and NiCoFeCrMn at fluence  $5 \times 10^{16}$  ions/cm<sup>2</sup> showing the effect of increasing the number of element on the swelling resistance. (b) Cross-sectional TEM image of 1.5 MeV irradiated Ni, NiFe, NiCo, and NiCoFeCr at fluence  $5 \times 10^{16}$  ions/cm<sup>2</sup> showing the effect of increasing the number of elements at a temperature 500°C, [Scale of 50 nm in the zoomed image in figure (b) is for both figure (a) and figure (b) and (c) Cross-sectional TEM image of 3.0 MeV irradiated NiCoFeCrMn and NiCoFeCrPd at fluence  $5 \times 10^{16}$  ions/cm<sup>2</sup> showing the effect of type of elements at a temperature 420°C, and 500°C. (Figure adapted from Ref.[66] under licence:<https://creativecommons.org/licenses/by/4.0/>).

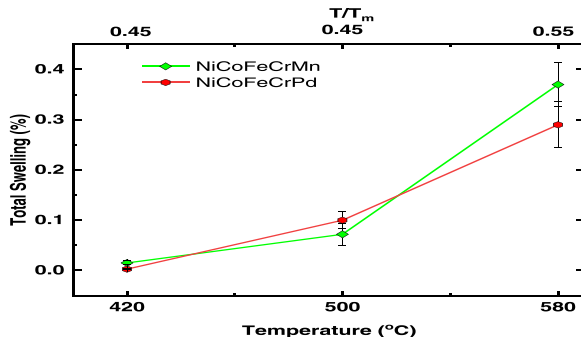


**Figure 7.** Variation of total void swelling percentage in NiCoFeCrMn and NiCoFeCrPd high entropy alloy irradiated with 3 MeV Ni ion to a fluence  $5 \times 10^{16}$  ions per cm<sup>2</sup> at temperatures of 420°C, 500°C and 580°C. (Figure adapted from Ref. [79] under licence:<https://creativecommons.org/licenses/by/4.0/>).

mechanical properties of the structural material start degrading and ultimately affect the lifetime of the structural material. This effect of the swelling has been observed in many in-situ TEM studies [87,88] and usually, the equation given in Ref. [89] is used to calculate the total swelling percentage from the TEM HAADF image. Lu *et al.* studied the effect of the compositional complexities of various materials (pure Ni, NiFe, NiCoFe and NiCoFeCrMn) by irradiating with Ni ion beam of two energies 3.0 MeV and 1.5 MeV to a fluence of  $5 \times 10^{16}$  ions/cm<sup>2</sup> and  $3 \times 10^{15}$  ions/cm<sup>2</sup>, respectively at a temperature of 773 K. The cross-sectional TEM result [Fig. 6(a-b)] shows that the total swelling percentage in Ni, NiFe, NiCoFe and NiCoFeCrMn are 9.4%, 0.45%, 0.15% and 0.1%, respectively. With the increase in the energy of the ion beam from 1.5 MeV to 3.0 MeV, the size of the voids increased for all alloy compositions and the defect clusters also moved deeper inside the sample shown in Fig. 6(a) as compared to the depth of defects in Fig. 6(b), but surprisingly the microstructures were not modified [26]. Similarly, irradiation-induced void swelling and void distribution in the same set of alloys are also investigated

by measuring the step height of the swelled region using a 3D optical profilometer. The step height calculated from the profilometer and the swelling obtained from TEM images were observed to be maximum for Ni compared to all other complex alloys NiCo, NiCoCr, and NiCoFeCrMn. Also, to their surprise, it was also noticed that the alloys containing Fe show an appreciable reduction in swelling for e.g. NiFe shows relatively less swelling (0.33%) than NiCoCr with (1.1%) swelling. Similarly, NiCoFe shows less swelling (0.2%) than NiCoCrFe with (0.33%) swelling in NiCoCrFe [76]. It is argued using the theoretical MD simulation that the migration pathway of the defect clusters in pure Ni is linear while it follows 3-dimensional pathways in distorted complex alloys, thus offering more recombination of interstitials in the case of complex alloys [26].

The dependence of the void swelling on the temperature is also investigated in the best swelling-resistant alloys NiCoFeCrMn (Mn-HEA) and NiCoFeCrPd (Pd-HEA) at temperatures 420°C(0.45  $T_m$ ), 500°C(0.50  $T_m$ ), and 580°C(0.55  $T_m$ ) is shown in Fig. 6(c). It is observed that the void size increases with the irradiation temperature for fixed energy and ion fluence. The total void swelling in Mn-HEA is larger than that of the Pd-HEA at 420°C whereas swelling is almost similar at intermediate temperature (500°C) but Pd-HEA shows much better swelling resistance at higher temperatures 580°C as shown in Fig. 7. Thus, these results show the retarded void growth in Pd-HEA compared to Mn-HEA, which is primarily attributed to the large size effect of Pd as it is reported that the large size atom offers trapping sites which increases the probability of vacancy-interstitial recombination and also produces pronounced lattice strain [68,74,90]. Based upon the above survey, the swelling resistance can be ranked as Pd-HEA > Mn-HEA  $\geq$  NiCoFe > NiCoFeCr  $\geq$  NiFe > NiCoCr = NiCo > Ni, which clearly indicates the improvement in the swelling resistance with alloys having more number of principal elements. A few exceptions like NiFe and NiCoFe having better swelling resistance than NiCoCr and NiCoCrFe show that the nature and size of the element are also important. These results suggest that the intrinsic nature of the element should also be taken into consideration for the new radiation-resistant alloys.

#### 4.2. Phase stability

It is desirable that materials exposed to energetic ions at elevated temperatures should be resistant to the formation of undesirable phases because it can change the chemical, physical and mechanical properties of the materials. The radiation-induced displacement cascade leads to the formation of the secondary phase. For example, embrittlement of Cr-steel takes place due to the formation of the Cr-rich  $\alpha$  phase which gets enhanced by radiation damage via accelerated diffusion of elements [91–93]. The radiation-induced phase separation in the austenitic stainless steel by the formation of Ni-rich and Si-rich phases in the matrix is also a point of concern in nuclear technology [94,95]. Precipitation of intermetallics like Ni-Si, Ni-Ge, and Ni-Be consisting of Ni-rich phase occurs at defect sinks after irradiation of alloys because the solute concentration exceeds the solubility limit at a given temperature through radiation-induced segregation (RIS) [96,97]. In the light water reactor (LWR), neutron-irradiation causes the formation of Cu-rich and (Ni-Mn-Si)-rich precipitates which limits the life extension of the reactor due to their resulting embrittlements [98,99]. Such kinds of precipitation take place due to the recombination of the vacancies and interstitials during irradiation [100,101]. Therefore, any undesirable phase change could lead to deterioration in important properties like loss of ductility and loss of corrosion resistance of the structure material. Kumar *et al.* investigated the phase stability of non equi-atomic Fe-NiCrMn (Ni 27 wt%, Fe 28 wt%, Cr 27 wt%, Mn 18 wt%) alloy under irradiation of 3 MeV and 5.8 MeV Ni ions with a dose range from 0.03 to 10 dpa in a temperature range of 25°C to 700°C. The alloy phase was found stable under these irradiation conditions, apart from the formation of precipitates of oxide rich in Cr and Mn. A small increase in dislocation loop size from 4 to 5.5 nm is also observed upon increase in the temperature from 400 °C to 700°C at a peak dose of 10 dpa [28]. Similarly,  $Al_xCoCrFeNi$  ( $x = 0.1, 0.75$  and  $1.5$  molar ratios) doped alloys were stable on irradiation with 3 MeV Au ions at a maximum dose of about 100 dpa apart from cluster precipitation in the case of 0.75 and 1.5 molar alloys [102]. In addition Yang *et al.* observed high phase stability of  $Al_{0.1}CoCrFeNi$  alloys on irradiation with 3 MeV Au ions in a high-temperature range of (250–650) °C [69].

Recently, a stable phase is also reported for CoCrFeNi and Al-doped  $Al_{0.12}CoCrFeNi$  alloys irradiated with Ni ions of about a dose of 100 dpa at a temperature of 500°C [103]. The TEM-SAED images of 0.12 molar Al-doped NiCoFeCr alloys show the formation of an additional phase apart from fcc matrix and the TEM dark field image shows the formation of nano-size secondary phase precipitates with an average size of 9 nm [Fig. 8(b)]. Thus, the stability of the Al-doped

HEAs is deteriorated due to the formation of secondary phases. However, Yang *et al.* [104] found great phase stability with no secondary phase in 0.1 molar Al-doped NiCoFeCr irradiation with 3 MeV Au ions to a fluence of  $1 \times 10^{16}$  ions/cm<sup>2</sup> ( $\approx 40$  dpa) at room temperature. The high phase stability in the alloy irradiated at room temperature is explained on the basis of the high configurational entropy and low mobility of defects at room temperature. They also reported precipitation behaviour in the Al-rich alloy (0.75 and 1.5 molar Al) which is attributed to the presence of Al and Ni enriched ordered B2 phase. The formation of precipitates also depends upon the ion fluence because there was no precipitation below  $5 \times 10^{15}$  ions/cm<sup>2</sup> fluence and it was increased with an increase in the ion fluence. Therefore, understanding the mechanism behind the formation of secondary phase formation on irradiation is necessary for the design of the radiation-resistant alloys. It is proposed that thermodynamic instability is created by positive binary mixing enthalpies which provide a driving force for the precipitation. This effect is observed in binary immiscible disordered alloys [105,106].

However, there are few cases where the precipitations don't take place and the phase remains stable, which is attributed to the higher configurational entropy competing against the thermodynamic driving force [69]. Another mechanism behind the precipitation is the role of precipitants themselves (e.g. Ni-Al intermetallic phase in Al added HEAs). The separation of NiMn phase in NiCoCrFeMn is explained on the basis of the high negative value of enthalpy of mixing between Ni-Al and Ni-Mn among the constituents. King *et al.* identified two parameters namely  $\delta$  and  $\phi$  for the prediction of phase stability. For a stable solid solution, the values of  $\delta$  and  $\phi$  are found to be  $\leq 6.6$  and  $\geq 1$ , respectively [44,107]. The values of  $\delta$  for both Ni-CoFeCr and  $Al_{0.12}NiCoFeCr$  come out to be 1.2 and 2.6, respectively which are smaller than expected values. The calculated values of  $\phi$  for pure and Al-doped NiCoFeCr alloy are 1.2 and 0.9, respectively suggesting that the Al-doped phase forms an unstable solid solution at the melting temperature. The formation of the stable solid solution takes place in most of the cases only when the atomic size difference is less than the critical value and the change in the Gibbs free energy is more than the maximum value of enthalpy for the formation of intermetallic of the constituent elements. Thus, radiation-induced phase separation is the sole reason for the phase instability under ion irradiation at high temperatures, which is discussed in the next section.

##### 4.2.1. Radiation-induced segregation

The radiation-induced segregation (RIS) is a phenomenon in which irradiation at high temperatures leads to the dragging of the solute against the vacancies movement created due to irradiation. In

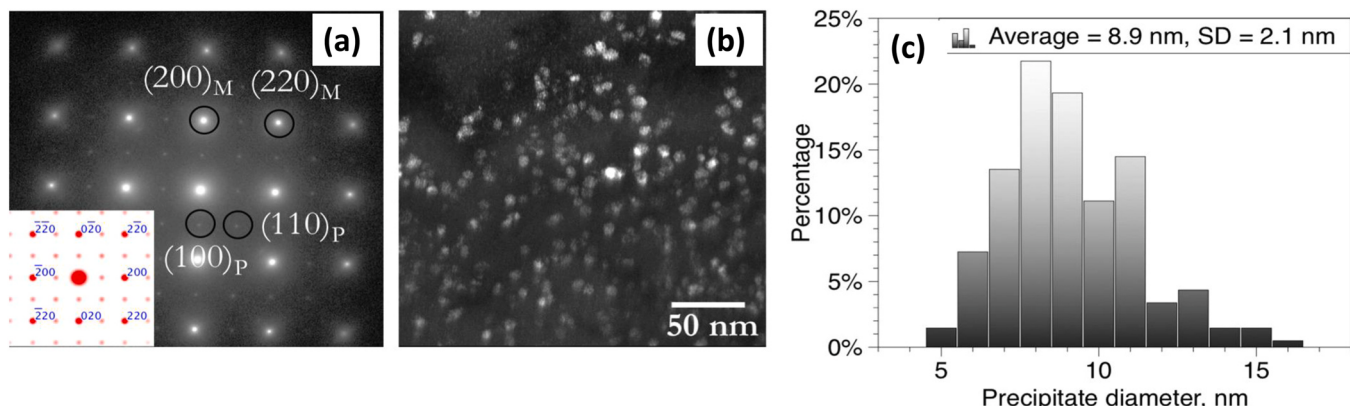


**Figure 8.** TEM images of Al-doped NiCoFeCr HEA  $Al_{0.12}$  NiCoFeCr show (a) the diffraction pattern of the irradiated matrix along [001] zone axis and in between some secondary phase intermetallic  $Ni_3Al$  (L1<sub>2</sub>) formation as marked by (p), (b) formation of precipitates due to irradiation in the dark-field image, (c) size distribution of the precipitates in the irradiated region.

(Figure adapted from Ref.[103] under licence:<https://creativecommons.org/licenses/by/4.0/>).

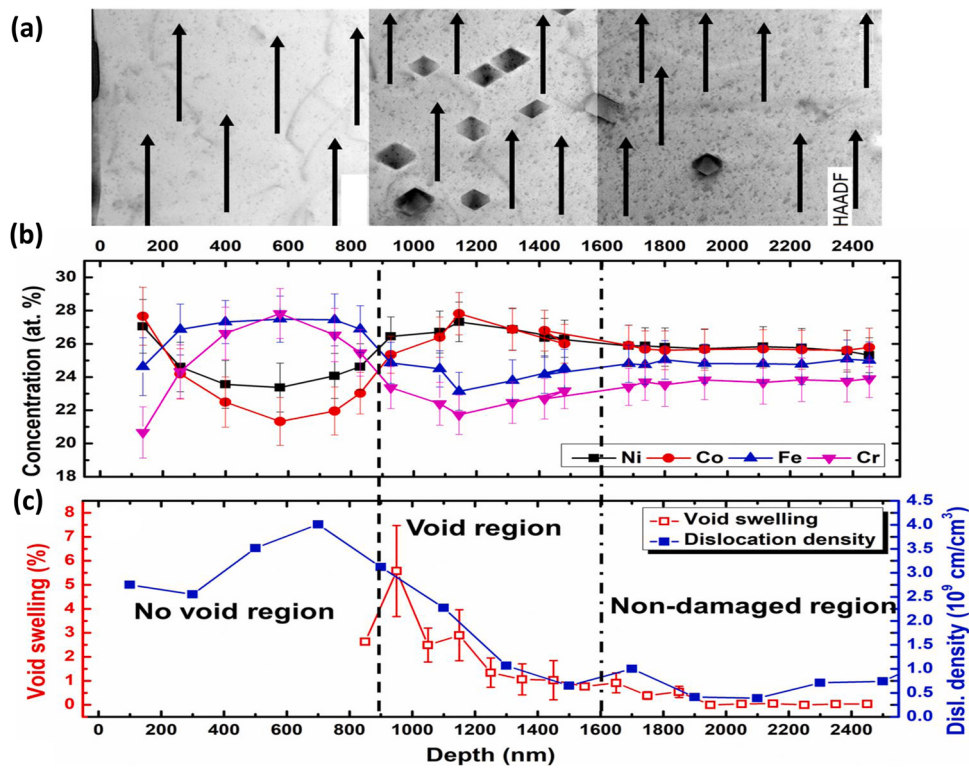


**Figure 9.** (a) TEM image of the different regions (b) change in concentration of various elements in different damage regions (c) void distribution in different damage region (Figure adapted from Ref. [113] under licence:<https://creativecommons.org/licenses/by/4.0/>).

the case of RIS, undesirable changes in the atomic concentration take place in the vicinity of large defects like dislocation loops, grain boundaries and voids, etc and thus causing the preferential moments of solute atoms at the defect site, ultimately degrades the mechanical properties in terms of hardening, embrittlement, and cracking of the materials being used in such environments [61,62]. The effect of RIS is found in the conventional stainless steel being used for the core of light water reactor, when irradiated with neutrons to several dpa at 300°C, [62]. The enrichment of smaller element Ni and the depletion of Cr were observed because of the preferential diffusion [62]. Generally, two theories are used to explain the mechanism behind the RIS, the inverse Kirkendall and solute drag mechanism, details of these mechanisms can be found elsewhere [108,109]. The enrichment of Ni in the NiCrMn and NiCrFe alloy explained on the basis of these theories suggests that the oversized elements caused the delay during diffusion, whereas the depletion of Cr and Mn is because undersized elements undergo faster diffusion [63,64,110]. Both these effects cause a change in concentration at the grain boundaries, dislocation loops and voids. It has been reported that, when the concentration of these elements increase beyond the solubility limit that causes instability of the phase of the matrix and forms unwanted intermetallic phases like NiAl and NiMn [111]. Theoretical Ab initio calculations suggest a larger contribution from the interstitial assisted diffusion of Cr in RIS than vacancy-assisted diffusion in binary NiCr alloy [65].

Experiment and modeling studies suggest that interstitial assisted diffusion contributes largely at low temperatures. But in the intermediate temperature (0.3–0.6)T<sub>m</sub> range, both the processes contribute to the diffusion process. Various reports on ion and electron irradiation found that the segregation of the constituents elements occurs mainly around the defects sites such as grain boundaries, dislocations and void, etc. [69,73,112]. Recently Zhe Fan et al. [113] studied the effect of 3 MeV Ni ion at 580°C to a fluence of 5 × 10<sup>16</sup> ions/cm<sup>2</sup> on RIS behaviour in NiCoCrFe HEA. They found the variation in the concentration at the site of defects as well as in the

matrix. In the shallow region, there is an enrichment of Cr and Co with depletion of Ni and Fe whereas in the void region, enrichment of Ni and Fe with depletion of Cr and Fe is observed. This shows that a non-void region is developed in the shallow region despite high damage due to the recombination of under-size elements Cr and Fe with the vacancies leading to Cr and Fe rich region as shown in Fig. 9(b). However, observation of the enrichment of Ni and Co with the depletion of Cr and Fe occur in the void region as shown in [Fig. 9(b)] is attributed to the higher vacancy migration energy for Ni (1.021) eV and Co (0.982) eV than (0.587) eV Cr and Fe (0.799) eV. In the Al<sub>0.1</sub>CoCrFeNi alloys on irradiation with 3 MeV Au ions in a high-temperature range of (250–650)°C, Yang et al. observed void formation, radiation-induced enrichment of Ni, Co and depletion of Fe, Cr at the boundaries of voids in the EDS elemental mapping studies [69]. But, the SAED pattern of NiCoFeCr alloy showed only a single phase fcc with no secondary phase suggesting that aluminium addition destabilizes the fcc matrix.

Similarly, Lu et al. [73] carried out irradiation with 3 MeV Ni<sup>+</sup> ions at 773 K to a fluence of 1 × 10<sup>16</sup> ions/cm<sup>2</sup>. From their studies in a series of Ni, NiFe, NiCoFe, NiCoCrFe and NiCoCrFeMn alloys, it is observed the enrichment of the Ni and Co and depletion Fe and Cr in the vicinity of loops. Although this effect is suppressed in the HEAs (NiCoCrFeMn, NiCoCrFe) as compared to other alloys [Fig. 10(a, b)]. However, opposite behaviour in RIS was observed on electron irradiation at 400°C upto 1 dpa in NiCoCrFeMn and NiCoCrFeMn. There is a huge Ni/Co enrichment and depletion of Pd/Mn in NiCoCrFeMn and NiCoCrFePd compared to NiCoCrFe [Fig. 10] which is explained on the basis of negative enthalpy of mixing NiMn and large positive enthalpy for Ni/CoPd leads to such deviations [114]. Thus, these results clearly show the different responses to ions and electron irradiation towards RIS. The ion irradiation also generates displacement [115] which suppresses the role of thermodynamic parameters e.g. ΔH compared to the atomic diffusion coupled with the migration of point defects and clusters which further modulates in HEAs. Therefore, irritation-induced segregation is based on the diffusion

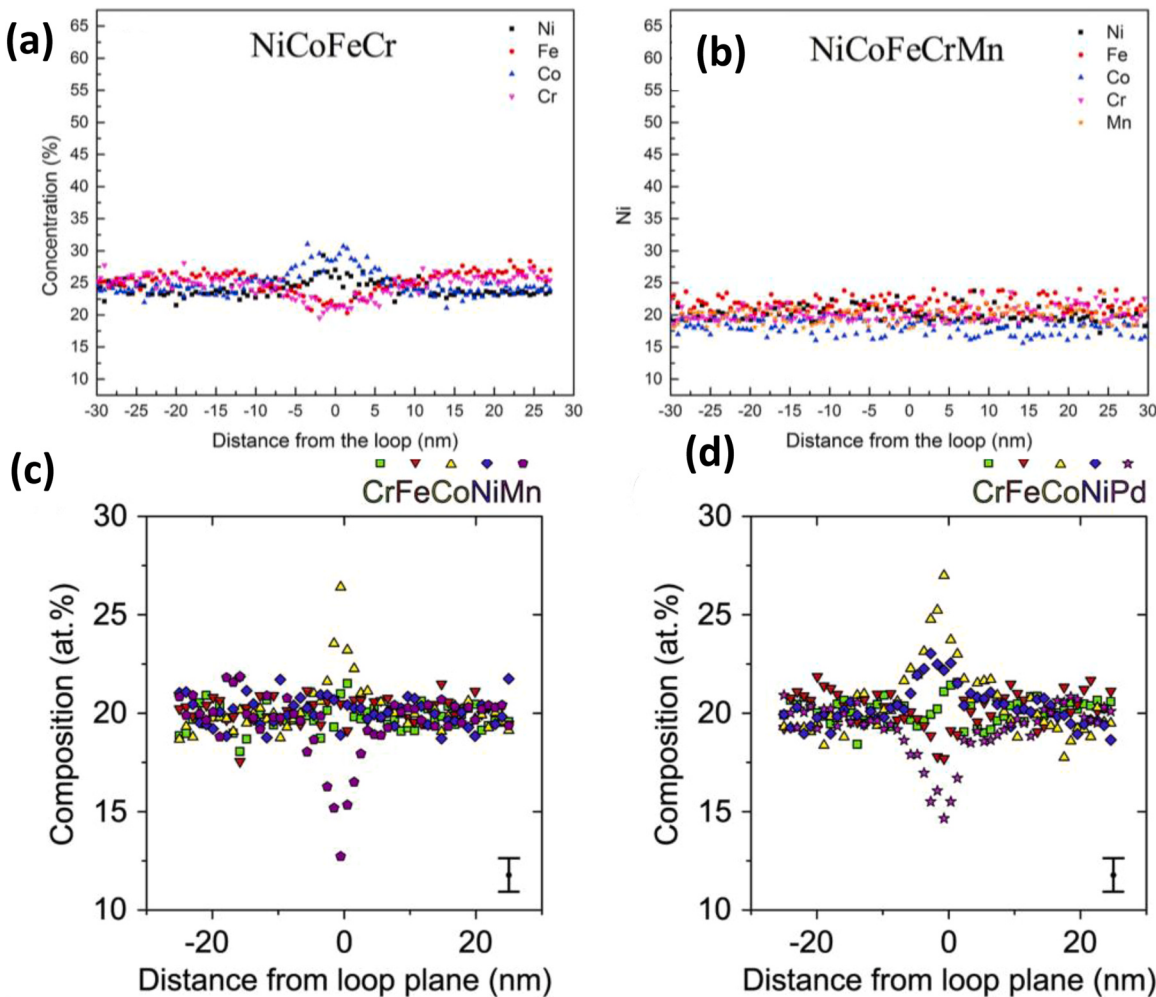


**Figure 10.** Atomic concentration variation at loop in (a) NiCoCrFe and (b) NiCoCrFeMn after 3 MeV  $\text{Ni}^{+2}$  ions at 773 K to a fluence  $1 \times 10^{16}$  ions/ $\text{cm}^2$  (c) atomic concentration variation at Frank loop in (a) NiCoCrFeMn and (d) NiCoCrFePd on 1250 kV electrons irradiation up to 1 dpa. (Figures adapted from Ref. [73,114] under licence:<https://creativecommons.org/licenses/by/4.0/>).

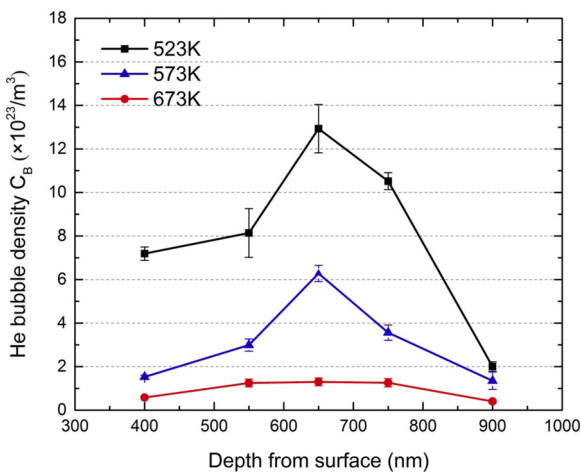


**Figure 11.** Variation in the density of bubbles with depth at different temperatures. (Figure adapted from Ref. [67] under licence:<https://creativecommons.org/licenses/by/4.0/>).

process which follows as  $D_{\text{Mn}} > D_{\text{Cr}} > D_{\text{Fe}} > D_{\text{Co}} > D_{\text{Ni}}$  in NiCoCrFeMn model system. It is based on the atomic size that shows depletion for faster diffusing elements and enrichment for slowest diffusing elements in the matrix [111,112]. Thus, RIS can be significantly reduced

by the careful selection of alloying elements to control the diffusion process and by reducing the interstitial migrations. Temperature-dependent RIS investigations in NiFeMnCr on irradiation with 3 MeV and 5.8 MeV Ni at a dose range in (0.03–10) dpa showed no RIS at 400°C, slight Ni enrichment at the intermediate temperature (500–600)°C, and reduction in solute segregation due to back diffusion of solute at 700°C [28]. Similar results were reported by Yang *et al.* on 3 MeV Au irradiation in AlNiCoCrFe where no precipitation at low temperature < 500°C, and the formation of B2 precipitation at 650°C was observed [116].

#### 4.3. Bubble formation

The bubble formation is yet another issue regarding the performance of the nuclear reactor operation. Since, inert gases such as He, Xe, and Kr are the by-products of  $(n,\alpha)$  nuclear transformation. These fission fragments are insoluble in the alloy matrix and form fission gases. These fission gases have a great influence on the thermal conductivity, and mechanical properties due to swelling and thus ultimately alter the neutron economy of the reactors [117,118].

In order to evaluate the performance of the HEAs against the bubble formation, HEAs are irradiated with  $\text{He}^+$  ions at elevated temperatures (400–700)°C. Chen *et al.* [67] showed suppression of the He bubble formation in FeCoNiCr HEA as compared to pure Ni and austenitic stainless steel on irradiation with  $\text{He}^+$  ions at

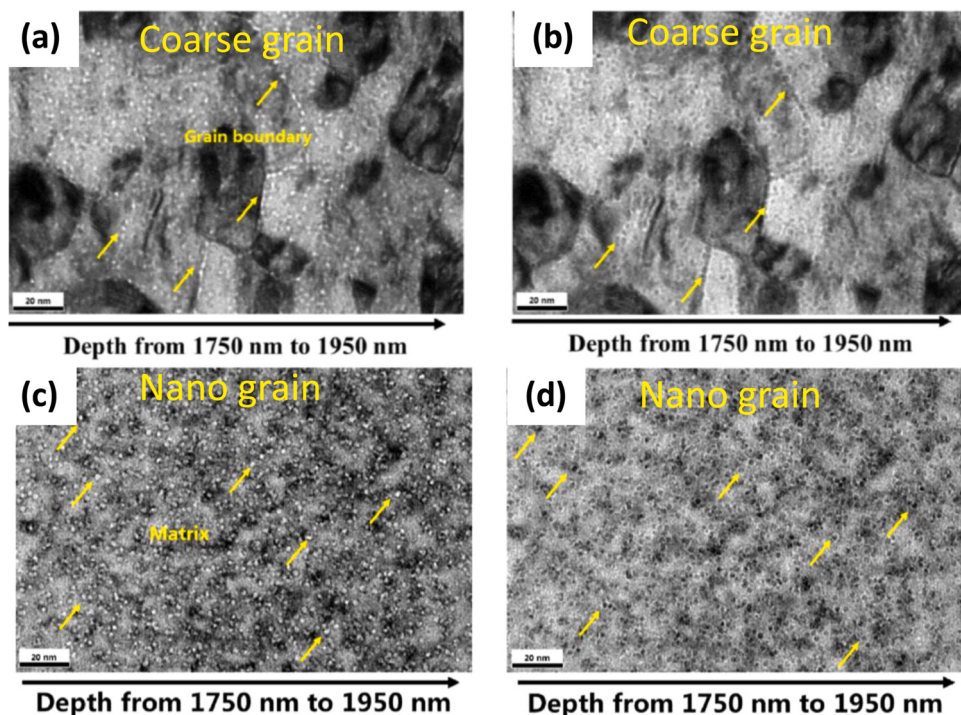


**Figure 12.** The bright field TEM images of bubble formation along the grain boundaries in coarse grain sized NiMoCr alloy at  $3 \times 10^{16}$  ions/cm<sup>2</sup> ion fluence at 650°C (a) under focused condition, (b) over-focus condition. Similar images for nano-grain sized NiMoCr alloy along the grain boundaries (c) under-focus condition, (d) over-focus condition. (Figure adapted from Ref. [122] under licence:<https://creativecommons.org/licenses/by/4.0/>).

temperatures 523 K, 573 K and 673 K. The temperature-dependent helium density distribution showed a reduction in the density of He with the increase in temperature [Fig. 11], which is attributed to the collapsing of the small bubbles to large bubbles owing to the enhancement of diffusion at high temperature. The activation energy for the He diffusion in HEAs ( $1.075 \pm 0.208$ ) eV is larger than 316 L stainless steel (0.98 eV) [119], owing to the sluggish diffusion effect in HEAs. Similar results were obtained by Yang et al. [120] on comparing the bubble size in NiCoCrFeMn HEA with 304SS and pure Ni after irradiated with He-ion both at RT and 450°C. The observed bubble size ( $4.0 \pm 0.9$ ) nm in HEAs is smaller than that of 304SS ( $5.3 \pm 1.0$ ) nm and pure Ni ( $6.7 \pm 1.0$ ) nm. Similarly in Ti and TiZrHfMoNb HEA films the bubble sizes were ( $2.54 \pm 0.46$ ) nm and ( $1.08 \pm 0.28$ ) nm, respectively with higher density in TiZrHfMoNb [121]. The presence of high-level lattice distortions and compositional complexities lead to modification in the activation energy, migration energy and the diffusion barrier in HEAs which results in reduced damage accumulation and suppression of bubble formation in HEAs. The effect of grain size on the bubble formation was studied by Zhu et al. by using 1 MeV He<sup>+</sup> ion irradiation at 650°C. It is observed that nano-grain sizes are more radiation tolerant and the size of bubbles increases with increases in the ion fluence [Fig. 12]. Also to their surprise at the same elevated temperature and irradiation condition, there was no irradiation induce dislocation or precipitation in the case of the nano-grain-sized sample. The observation of smaller bubble size is explained on the basis of trapping of He atoms at grain boundaries as well as presence for a longer duration in the nano-grain-sized sample thus delaying the bubble growth [122].

## 5. Conclusions

The paper summarizes various aspects of HEAs applicability as the structural materials in terms of various radiation-induced phenomena under different conditions both at room temperature and elevated temperatures with more focus on the following:

1. Critical parameters to design a radiation-resistant alloy.
2. Creation of radiation-induced defect and their dynamics at room temperature and elevated temperature.
3. Phase stability, swellings, RIS, bubble formation and their evolution at high-temperature irradiation conditions.

It is found that HEAs or multi-component alloys are more radiation resistant compared to conventional alloys. The radiation-resistance response critically depends on the microstructure, local disorder, concentration, type, size of the alloying element and number of alloying elements. It is also noticed that Pd-containing alloys exhibit exceptional resistance to radiation among the studied alloys. RBS-sputtering yield and EXAFS studies showed that Pd-containing alloys have lesser damage due to large chemical inhomogeneity and the highest local lattice distortion produced by Pd. TEM investigation confirmed that the defect size or the dislocation size is larger in pure metals than in their binary or ternary alloys. The size of dislocation is further reduced in the case of Pd-containing alloys. This signifies that large atoms produce a high hindrance to defect mobility due to the production of significant lattice distortion.

Therefore, one of the best ways to design radiation-resistant alloys is by the careful selection of alloying elements which produce strong lattice distortion and short-range ordering. The presence of strong lattice distortion and SRO hinders defect mobility by trapping and avoiding the accumulation of vacancies. Moreover, the phase stability, RIS and bubble formation at high-temperature irradiation can be modulated by changing the type of alloying elements, grain size and microstructure.

## 6. Future scope

Currently, austenitic steels are widely used as structural materials in various water-cooled nuclear fission reactors. Future Gen-IV reactors require excellent resistance to radiation up to a dose of 200 dpa and temperatures up to 900°C [8,59,123,124]. But, currently

used austenitic stainless steel and Fe-based austenitic stainless steel in the nuclear energy systems suffer from various radiation-induced mechanical failures due to the formation of cracking, corrosion, fractures, void swelling and RIS at elevated temperatures [8,125]. Among these, voids swelling and RIS are two extremely important challenges for the materials exposed to energetic ions at elevated temperatures. Such phenomena lead to an unacceptable dimensional change with the span of time causing mechanical and thermal degradation [126], whereas RIS can cause phase instability, embrittlement, and stress corrosion cracking issues [61,62]. The above-mentioned issues can be solved by the use of HEAs or multi-component alloys. Several HEAs show superior resistance to various irradiation-induced phenomena at elevated temperatures although, their phase stability for a longer period of time at elevated temperatures may be objectionable due to the formation of the brittle intermetallics compounds among the constituents of HEAs [10,127–129]. Beside these, HEAs have several other mechanical and physical properties e.g. high strength, wear resistance and corrosion resistance at elevated temperatures. These properties make HEAs a potential candidates for high temperature fission or fusion structural applications. It is speculated that high configurational entropy could also influence point defect recombination phenomena in irradiated alloys by modifying the vacancy-interstitial recombination interaction distance, solute diffusivity, or other mechanisms, thereby making HEAs superior radiation stability compared to conventional single-phase alloys.

## CRediT authorship contribution statement

**Abid Hussain:** Conceptualization, Writing – original draft. **R.S. Dhaka:** Editing and review. **Ho Jin Ryu:** Validation. **Saurabh Kumar Sharma:** Manuscript corrections. **Pawan Kumar Kulriya:** Supervision, conceptualization of this study, Methodology.

## Data Availability

Data will be made available on request.

## Declaration of Competing Interest

The authors declare that they have no known competing financial interests or personal relationships that could have appeared to influence the work reported in this paper.

## Acknowledgement

One of the authors, A.H. is thankful to UGC for awarding Junior Research Fellowship with reference no. 1330/(CSIR-UGC NET DEC. 2017). One of the authors, (P.K.K.) acknowledges the Board of Research in Nuclear Sciences (BRNS) for providing financial support under the project 58/14/05/2019- BRNS/37-013 and also R.S.D. acknowledges the BRNS for supporting with an Arc melting system through DAE Yong Scientist Research Award (Project Sanction No. 24/20/12/2015/BRNS).

## References

- [1] J.-W. Yeh, S.-K. Chen, S.-J. Lin, J.-Y. Gan, T.-S. Chin, T.-T. Shun, C.-H. Tsau, S.-Y. Chang, Nanostructured high-entropy alloys with multiple principal elements: novel alloy design concepts and outcomes, *Adv. Eng. Mater.* 6 (5) (2004) 299–303.
- [2] K.-Y. Tsai, M.-H. Tsai, J.-W. Yeh, Sluggish diffusion in co-cr-fe-mn-ni high-entropy alloys, *Acta Mater.* 61 (13) (2013) 4887–4897.
- [3] W. Zhang, P.K. Liaw, Y. Zhang, Science and technology in high-entropy alloys, *Sci. China Mater.* 61 (1) (2018) 2–22.
- [4] Z. Tang, M.C. Gao, H. Diao, T. Yang, J. Liu, T. Zuo, Y. Zhang, Z. Lu, Y. Cheng, Y. Zhang, et al., Aluminum alloying effects on lattice types, microstructures, and mechanical behavior of high-entropy alloys systems, *Jom* 65 (12) (2013) 1848–1858.
- [5] S.J. Zinkle, L.L. Snead, Designing radiation resistance in materials for fusion energy, *Annu. Rev. Mater. Res.* 44 (2014) 241–267.
- [6] R. Dhaka, C. Biswas, A. Shukla, S. Barman, A. Chakrabarti, Xe and ar nanobubbles in al studied by photoemission spectroscopy, *Phys. Rev. B* 77 (10) (2008) 104119.
- [7] R. Dhaka, S. Barman, Bimodal distribution of neon nanobubbles in aluminum, *Phys. Rev. B* 79 (12) (2009) 125409.
- [8] S.J. Zinkle, G. Was, Materials challenges in nuclear energy, *Acta Mater.* 61 (3) (2013) 735–758.
- [9] Z. Wu, H. Bei, G.M. Pharr, E.P. George, Temperature dependence of the mechanical properties of equiatomic solid solution alloys with face-centered cubic crystal structures, *Acta Mater.* 81 (2014) 428–441.
- [10] C.-M. Lin, H.-L. Tsai, Equilibrium phase of high-entropy feconicrcu0.5 alloy at elevated temperature, *J. Alloy. Compd.* 489 (1) (2010) 30–35.
- [11] X. Chen, Q. Wang, Z. Cheng, M. Zhu, H. Zhou, P. Jiang, L. Zhou, Q. Xue, F. Yuan, J. Zhu, et al., Direct observation of chemical short-range order in a medium-entropy alloy, *Nature* 592 (7856) (2021) 712–716.
- [12] F. Zhang, S. Zhao, K. Jin, H. Xue, G. Velisa, H. Bei, R. Huang, J. Ko, D. Pagan, J. Neufeind, et al., Local structure and short-range order in a nicocr solid solution alloy, *Phys. Rev. Lett.* 118 (20) (2017) 205501.
- [13] J.B. Seol, J.W. Bae, J.G. Kim, H. Sung, Z. Li, H.H. Lee, S.H. Shim, J.H. Jang, W.-S. Ko, S.I. Hong, et al., Short-range order strengthening in boron-doped high-entropy alloys for cryogenic applications, *Acta Mater.* 194 (2020) 366–377.
- [14] D. Liu, Q. Wang, J. Wang, X. Chen, P. Jiang, F. Yuan, Z. Cheng, E. Ma, X. Wu, Chemical short-range order in fe50mn30co10cr10 high-entropy alloy, *Mater. Today Nano* 16 (2021) 100139.
- [15] L. Zhou, Q. Wang, J. Wang, X. Chen, P. Jiang, H. Zhou, F. Yuan, X. Wu, Z. Cheng, E. Ma, Atomic-scale evidence of chemical short-range order in crconi medium-entropy alloy, *Acta Mater.* 224 (2022) 117490.
- [16] Q. Pan, L. Zhang, R. Feng, Q. Lu, K. An, A.C. Chuang, J.D. Poplawsky, P.K. Liaw, L. Lu, Gradient cell-structured high-entropy alloy with exceptional strength and ductility, *Science* 374 (6570) (2021) 984–989.
- [17] J. Wang, P. Jiang, F. Yuan, X. Wu, Chemical medium-range order in a medium-entropy alloy, *Nat. Commun.* 13 (1) (2022) 1021.
- [18] R. Zhang, S. Zhao, J. Ding, Y. Chong, T. Jia, C. Ophus, M. Asta, R.O. Ritchie, A.M. Minor, Short-range order and its impact on the crconi medium-entropy alloy, *Nature* 581 (7808) (2020) 283–287.
- [19] S. Zhao, Role of chemical disorder and local ordering on defect evolution in high-entropy alloys, *Phys. Rev. Mater.* 5 (10) (2021) 103604.
- [20] O.K. Orhan, M. Hendy, M. Ponga, Electronic effects on the radiation damage in high-entropy alloys, *Acta Mater.* 244 (2023) 118511.
- [21] S.K. Sharma, V. Grover, A. Tyagi, D. Avasthi, U. Singh, P. Kulriya, Probing the temperature effects in the radiation stability of nd2zr2o7 pyrochlore under swift ion irradiation, *Materialia* 6 (2019) 100317.
- [22] C. Nandi, V. Grover, P. Kulriya, A. Poswal, A. Prakash, K. Khan, D. Avasthi, A. Tyagi, Structural response of nd-stabilized zirconia and its composite under extreme conditions of swift heavy ion irradiation, *J. Nucl. Mater.* 499 (2018) 216–224.
- [23] M. Gupta, P. Kulriya, R. Meena, S. Neumeier, S. Ghumman, Probing swift heavy ion irradiation damage in nd-doped zirconolite, *Nucl. Instrum. Methods Phys. Res. Sect. B Beam Interact. Mater. At.* 453 (2019) 22–27.
- [24] A. Kumar, P. Kulriya, S. Sharma, V. Grover, A. Tyagi, V. Shukla, Structural and compositional effects on the electronic excitation induced phase transformations in gd2ti2-yzry7 pyrochlore, *J. Nucl. Mater.* (2020) 152278.
- [25] C.L. Dube, P.K. Kulriya, D. Dutta, P.K. Pujari, Y. Patil, M. Mehta, P. Patel, S.S. Khirwadkar, Positron annihilation lifetime measurement and x-ray analysis on 120 mev au+7 irradiated polycrystalline tungsten, *J. Nucl. Mater.* 467 (2015) 406–412.
- [26] C. Lu, L. Niu, N. Chen, K. Jin, T. Yang, P. Xiu, Y. Zhang, F. Gao, H. Bei, S. Shi, et al., Enhancing radiation tolerance by controlling defect mobility and migration pathways in multicomponent single-phase alloys, *Nat. Commun.* 7 (1) (2016) 1–8.
- [27] Y. Zhang, G.M. Stocks, K. Jin, C. Lu, H. Bei, B.C. Sales, L. Wang, L.K. Béland, R.E. Stoller, G.D. Samolyuk, et al., Influence of chemical disorder on energy dissipation and defect evolution in concentrated solid solution alloys, *Nat. Commun.* 6 (1) (2015) 1–9.
- [28] N.K. Kumar, C. Li, K. Leonard, H. Bei, S. Zinkle, Microstructural stability and mechanical behavior of fe nimncr high entropy alloy under ion irradiation, *Acta Mater.* 113 (2016) 230–244.
- [29] C. Lu, T. Yang, K. Jin, G. Velisa, P. Xiu, M. Song, Q. Peng, F. Gao, Y. Zhang, H. Bei, et al., Enhanced void swelling in nicofercpd high-entropy alloy by indentation-induced dislocations, *Mater. Res. Lett.* 6 (10) (2018) 584–591.
- [30] F. Zhang, S. Zhao, K. Jin, H. Bei, D. Popov, C. Park, J.C. Neufeind, W.J. Weber, Y. Zhang, Pressure-induced fcc to hcp phase transition in ni-based high entropy solid solution alloys, *Appl. Phys. Lett.* 110 (1) (2017) 011902.
- [31] S. Xia, X. Yang, T. Yang, S. Liu, Y. Zhang, Irradiation resistance in al x cocrfe ni high entropy alloys, *Jom* 67 (10) (2015) 2340–2344.
- [32] C. Zhang, F. Zhang, H. Diao, M.C. Gao, Z. Tang, J.D. Poplawsky, P.K. Liaw, Understanding phase stability of al-co-cr-fe-ni high entropy alloys, *Mater. Des.* 109 (2016) 425–433.
- [33] W.-R. Wang, W.-L. Wang, S.-C. Wang, Y.-C. Tsai, C.-H. Lai, J.-W. Yeh, Effects of al addition on the microstructure and mechanical property of alxcocrfe ni high-entropy alloys, *Intermetallics* 26 (2012) 44–51.

- [34] S. Haas, M. Mosbacher, O.N. Senkov, M. Feuerbacher, J. Freudenberger, S. Gezgin, R. Völk, U. Glatzel, Entropy determination of single-phase high entropy alloys with different crystal structures over a wide temperature range, *Entropy* 20 (9) (2018) 654.
- [35] F. Otto, Y. Yang, H. Bei, E.P. George, Relative effects of enthalpy and entropy on the phase stability of equiatomic high-entropy alloys, *Acta Mater.* 61 (7) (2013) 2628–2638.
- [36] M.G. Poletti, L. Battezzati, Electronic and thermodynamic criteria for the occurrence of high entropy alloys in metallic systems, *Acta Mater.* 75 (2014) 297–306.
- [37] D. Ma, B. Grabowski, F. Körmann, J. Neugebauer, D. Raabe, Ab initio thermodynamics of the cocrfemnni high entropy alloy: Importance of entropy contributions beyond the configurational one, *Acta Mater.* 100 (2015) 90–97.
- [38] G. Sheng, C.T. Liu, Phase stability in high entropy alloys: formation of solid-solution phase or amorphous phase, *Prog. Nat. Sci.: Mater. Int.* 21 (6) (2011) 433–446.
- [39] B. Schuh, F. Mendez-Martin, B. Völker, E.P. George, H. Clemens, R. Pippal, A. Hohenwarter, Mechanical properties, microstructure and thermal stability of a nanocrystalline cocrfemnni high-entropy alloy after severe plastic deformation, *Acta Mater.* 96 (2015) 258–268.
- [40] E. Pickering, R. Muñoz-Moreno, H. Stone, N. Jones, Precipitation in the equiatomic high-entropy alloy crmnfeconi, *Scr. Mater.* 113 (2016) 106–109.
- [41] F. Otto, A. Dlouhy, K.G. Pradeep, M. Kubenová, D. Raabe, G. Eggeler, E.P. George, Decomposition of the single-phase high-entropy alloy crmnfeconi after prolonged anneals at intermediate temperatures, *Acta Materialia* 112 (2016), pp. 40–52.
- [42] B. Schuh, B. Völker, J. Todt, N. Schell, L. Perrière, J. Li, J. Couzinié, A. Hohenwarter, Thermodynamic instability of a nanocrystalline, single-phase tizrbhfta alloy and its impact on the mechanical properties, *Acta Mater.* 142 (2018) 201–212.
- [43] D. Ma, M. Yao, K.G. Pradeep, C.C. Tasan, H. Springer, D. Raabe, Phase stability of non-equiatomic cocrfemnni high entropy alloys, *Acta Mater.* 98 (2015) 288–296.
- [44] X. Yang, Y. Zhang, Prediction of high-entropy stabilized solid-solution in multi-component alloys, *Mater. Chem. Phys.* 132 (2–3) (2012) 233–238.
- [45] S. Guo, C. Ng, J. Lu, C. Liu, Effect of valence electron concentration on stability of fcc or bcc phase in high entropy alloys, *J. Appl. Phys.* 109 (10) (2011) 103505.
- [46] H. Diao, R. Feng, K.A. Dahmen, P. Liaw, Fundamental deformation behavior in high-entropy alloys: an overview, *Curr. Opin. Solid State Mater. Sci.* 21 (5) (2017) 252–266.
- [47] Y. Lu, Y. Dong, S. Guo, L. Jiang, H. Kang, T. Wang, B. Wen, Z. Wang, J. Jie, Z. Cao, et al., A promising new class of high-temperature alloys: eutectic high-entropy alloys, *Sci. Rep.* 4 (2014) 6200.
- [48] Y. Dong, L. Jiang, H. Jiang, Y. Lu, T. Wang, T. Li, Effects of annealing treatment on microstructure and hardness of bulk alcrfenimo.0.2 eutectic high-entropy alloy, *Mater. Des.* 82 (2015) 91–97.
- [49] H. Jiang, H. Zhang, T. Huang, Y. Lu, T. Wang, T. Li, Microstructures and mechanical properties of co2moxni2vwx eutectic high entropy alloys, *Mater. Des.* 109 (2016) 539–546.
- [50] X. Wang, W. Zhai, J. Wang, B. Wei, Strength and ductility enhancement of high-entropy feconi2al0.9 alloy by ultrasonically refining eutectic structures, *Scr. Mater.* 225 (2023) 115154.
- [51] R.K. Nutor, Q. Cao, R. Wei, Q. Su, G. Du, X. Wang, F. Li, D. Zhang, J.-Z. Jiang, A dual-phase alloy with ultrahigh strength-ductility synergy over a wide temperature range, *Sci. Adv.* 7 (34) (2021) eabi4404.
- [52] C.-W. Tsai, M.-H. Tsai, J.-W. Yeh, C.-C. Yang, Effect of temperature on mechanical properties of al0.5cocrfeni wrought alloy, *J. Alloy. Compd.* 490 (1–2) (2010) 160–165.
- [53] O.N. Senkov, G. Wilks, J. Scott, D.B. Miracle, Mechanical properties of nb25mo25ta25w25 and v20nb20mo20ta20w20 refractory high entropy alloys, *Intermetallics* 19 (5) (2011) 698–706.
- [54] F. Yang, L. Wang, Z. Wang, Q. Wu, K. Zhou, X. Lin, W. Huang, Ultra strong and ductile eutectic high entropy alloy fabricated by selective laser melting, *J. Mater. Sci. Technol.* 106 (2022) 128–132.
- [55] Q. Ding, Y. Zhang, X. Chen, X. Fu, D. Chen, S. Chen, L. Gu, F. Wei, H. Bei, Y. Gao, et al., Tuning element distribution, structure and properties by composition in high-entropy alloys, *Nature* 574 (7777) (2019) 223–227.
- [56] S. Zinkle, G. Was, Materials challenges in nuclear energy, *Acta Mater.* 61 (3) (2013) 735–758.
- [57] R. Dhaka, K. Gururaj, S. Abhaya, G. Amarendra, S. Amirthapandian, B. Panigrahi, K. Nair, N. Lalla, S. Barman, Depth-resolved positron annihilation studies of argon nanobubbles in aluminum, *J. Appl. Phys.* 105 (5) (2009) 054304.
- [58] R. Dhaka, S. Barman, X-ray photoemission studies on rare gas bubbles in aluminium with annealing temperature, *Surf. Coat. Technol.* 203 (17–18) (2009) 2380–2382.
- [59] H. Chung, et al., Assessment of void swelling in austenitic stainless steel pwr core internals., Tech. rep., Argonne National Lab.(ANL), Argonne, IL (United States) (2006).
- [60] B. Singh, S. Zinkle, Defect accumulation in pure fcc metals in the transient regime: a review, *J. Nucl. Mater.* 206 (2–3) (1993) 212–229.
- [61] E.A. Kenik, J.T. Busby, Radiation-induced degradation of stainless steel light water reactor internals, *Mater. Sci. Eng.: R: Rep.* 73 (7–8) (2012) 67–83.
- [62] S.M. Bruemmer, E.P. Simonen, P.M. Scott, P.L. Andresen, G.S. Was, J.L. Nelson, Radiation-induced material changes and susceptibility to intergranular failure of light-water-reactor core internals, *J. Nucl. Mater.* 274 (3) (1999) 299–314.
- [63] T. Allen, J. Busby, G. Was, E. Kenik, On the mechanism of radiation-induced segregation in austenitic fe–cr–ni alloys, *J. Nucl. Mater.* 255 (1) (1998) 44–58.
- [64] A.J. Ardell, P. Bellon, Radiation-induced solute segregation in metallic alloys, *Curr. Opin. Solid State Mater. Sci.* 20 (3) (2016) 115–139.
- [65] G.S. Was, J.P. Wharry, B. Frisbie, B.D. Wirth, D. Morgan, J.D. Tucker, T.R. Allen, Assessment of radiation-induced segregation mechanisms in austenitic and ferritic–martensitic alloys, *J. Nucl. Mater.* 411 (1–3) (2011) 41–50.
- [66] K. Jin, C. Lu, L. Wang, J. Qu, W. Weber, Y. Zhang, H. Bei, Effects of compositional complexity on the ion-irradiation induced swelling and hardening in ni-containing equiatomic alloys, *Scr. Mater.* 119 (2016) 65–70.
- [67] D. Chen, Y. Tong, H. Li, J. Wang, Y. Zhao, A. Hu, J. Kai, Helium accumulation and bubble formation in feconicr alloy under high fluence he+ implantation, *J. Nucl. Mater.* 501 (2018) 208–216.
- [68] Y. Tong, K. Jin, H. Bei, J. Ko, D.C. Pagan, Y. Zhang, F. Zhang, Local lattice distortion in nicocr, feconicr and feconicrmn concentrated alloys investigated by synchrotron x-ray diffraction, *Mater. Des.* 155 (2018) 1–7.
- [69] T. Yang, S. Xia, W. Guo, R. Hu, J.D. Poplawsky, G. Sha, Y. Fang, Z. Yan, C. Wang, C. Li, et al., Effects of temperature on the irradiation responses of al0.1cocrfeni high entropy alloy, *Scr. Mater.* 144 (2018) 31–35.
- [70] C. Lu, K. Jin, L.K. Béland, F. Zhang, T. Yang, L. Qiao, Y. Zhang, H. Bei, H.M. Christen, R.E. Stoller, et al., Direct observation of defect range and evolution in ion-irradiated single crystalline ni and ni binary alloys, *Sci. Rep.* 6 (2016) 19994.
- [71] F. Granberg, K. Nordlund, M.W. Ullah, K. Jin, C. Lu, H. Bei, L. Wang, F. Djurabekova, W. Weber, Y. Zhang, Mechanism of radiation damage reduction in equiatomic multicomponent single phase alloys, *Phys. Rev. Lett.* 116 (13) (2016) 135504.
- [72] Y. Zhang, K. Jin, H. Xue, C. Lu, R.J. Olsen, L.K. Béland, M.W. Ullah, S. Zhao, H. Bei, D.S. Aidhy, et al., Influence of chemical disorder on energy dissipation and defect evolution in advanced alloys, *J. Mater. Res.* 31 (16) (2016).
- [73] C. Lu, T. Yang, K. Jin, N. Gao, P. Xiu, Y. Zhang, F. Gao, H. Bei, W.J. Weber, K. Sun, et al., Radiation-induced segregation on defect clusters in single-phase concentrated solid-solution alloys, *Acta Mater.* 127 (2017) 98–107.
- [74] Y. Tong, G. Velisa, T. Yang, K. Jin, C. Lu, H. Bei, J. Ko, D. Pagan, R. Huang, Y. Zhang, et al., Probing local lattice distortion in medium-and high-entropy alloys, arXiv preprint arXiv:1707.07745 (2017).
- [75] X. Wang, K. Jin, D. Chen, H. Bei, Y. Wang, W.J. Weber, Y. Zhang, K.L. More, Effects of fe concentration on helium bubble formation in niifex single-phase concentrated solid solution alloys, *Materialia* 5 (2019) 100183.
- [76] K. Jin, W. Guo, C. Lu, M.W. Ullah, Y. Zhang, W.J. Weber, L. Wang, J.D. Poplawsky, H. Bei, Effects of fe concentration on the ion-irradiation induced defect evolution and hardening in ni-fe solid solution alloys, *Acta Mater.* 121 (2016) 365–373.
- [77] F.X. Zhang, K. Jin, S. Zhao, S. Mu, H. Bei, J.C. Liu, H.Z. Xue, D. Popov, C. Park, G.M. Stocks, et al., X-ray absorption investigation of local structural disorder in ni1-xfx (x= 0.10, 0.20, 0.35, and 0.50) alloys, *J. Appl. Phys.* 121 (16) (2017) 165105.
- [78] F. Zhang, M.W. Ullah, S. Zhao, K. Jin, Y. Tong, G. Velisa, H. Xue, H. Bei, R. Huang, C. Park, et al., Local structure of nifpd solid solution alloys and its response to ion irradiation, *J. Alloy. Compd.* 755 (C) (2018).
- [79] T.-N. Yang, C. Lu, G. Velisa, K. Jin, P. Xiu, Y. Zhang, H. Bei, L. Wang, Influence of irradiation temperature on void swelling in nicofermn and nicoferpd, *Scr. Mater.* 158 (2019) 57–61.
- [80] F. Zhang, Y. Tong, G. Velisa, H. Bei, W. Weber, Y. Zhang, Local structure of ni80×20 (x: Cr, Mn, Pd) solid-solution alloys and its response to ion irradiation, *J. Phys.: Condens. Matter* 32 (7) (2019) 074002.
- [81] F. Zhang, Y. Tong, K. Jin, H. Bei, W.J. Weber, Y. Zhang, Lattice distortion and phase stability of pd-doped nicofer solid-solution alloys, *Entropy* 20 (12) (2018) 900.
- [82] A. Hussain, S. Khan, S.K. Sharma, K. Sudarshan, S.K. Sharma, C. Singh, P.K. Kulriya, Influence of defect dynamics on the nanoindentation hardness in nicoferpd high entropy alloy under high dose xe+ 3 irradiation, *Mater. Sci. Eng.: A* 863 (2023) 144523.
- [83] X.-M. Bai, A.F. Voter, R.G. Hoagland, M. Nastasi, B.P. Uberuaga, Efficient annealing of radiation damage near grain boundaries via interstitial emission, *Science* 327 (5973) (2010) 1631–1634.
- [84] C.M. Barr, N. Li, B.L. Boyce, K. Hattar, Examining the influence of grain size on radiation tolerance in the nanocrystalline regime, *Appl. Phys. Lett.* 112 (18) (2018) 181903.
- [85] S. Liu, W. Lin, Y. Zhao, D. Chen, G. Yeli, F. He, J.J. Kai, Effect of silicon addition on the microstructures, mechanical properties and helium irradiation resistance of NiCoCr-based medium-entropy alloys, *J. Alloy. Compd.* 844 (2020) 156162.
- [86] N. Kumar, M. Fusco, M. Komarasamy, R. Mishra, M. Bourham, K. Murty, Understanding effect of 3.5 wt% nacl on the corrosion of al0.1cocrfeni high-entropy alloy, *J. Nucl. Mater.* 495 (2017) 154–163.
- [87] K. Arakawa, K. Ono, M. Isshiki, K. Mimura, M. Uchikoshi, H. Mori, Observation of the one-dimensional diffusion of nanometer-sized dislocation loops, *Science* 318 (5852) (2007) 956–959.
- [88] Y. Matsukawa, S.J. Zinkle, One-dimensional fast migration of vacancy clusters in metals, *Science* 318 (5852) (2007) 959–962.
- [89] M.B. Toloczko, F. Garner, V. Voyevodin, V. Bryk, O. Borodin, V. Mel'Nychenko, A. Kalchenko, Ion-induced swelling of ods ferritic alloy ma957 tubing to 500 dpa, *J. Nucl. Mater.* 453 (1–3) (2014) 323–333.
- [90] T.-n. Yang, C. Lu, G. Velisa, K. Jin, P. Xiu, M.L. Crespiello, Y. Zhang, H. Bei, L. Wang, Effect of alloying elements on defect evolution in ni-20x binary alloys, *Acta Mater.* 151 (2018) 159–168.

- [91] M. Bachhav, G.R. Odette, E.A. Marquis,  $\alpha$  precipitation in neutron-irradiated fe-cr alloys, *Scr. Mater.* 74 (2014) 48–51.
- [92] K.G. Field, K.C. Littrell, S.A. Briggs, Precipitation of  $\alpha$  in neutron irradiated commercial fecrali alloys, *Scr. Mater.* 142 (2018) 41–45.
- [93] M. Mathon, Y. De Carlan, G. Geoffroy, X. Averty, A. Alamo, C. De Novion, A sans investigation of the irradiation-enhanced  $\alpha$ - $\alpha$  phase separation in 7–12 cr martensitic steels, *J. Nucl. Mater.* 312 (2–3) (2003) 236–248.
- [94] H. Brager, F. Garner, Swelling as a consequence of gamma prime ( $\gamma'$ ) and m23 (c, si) 6 formation in neutron irradiated 316 stainless steel, *J. Nucl. Mater.* 73 (1) (1978) 9–19.
- [95] Z. Jiao, G. Was, Novel features of radiation-induced segregation and radiation-induced precipitation in austenitic stainless steels, *Acta Mater.* 59 (3) (2011) 1220–1238.
- [96] A. Barbu, A. Ardell, Irradiation-induced precipitation in ni-si alloys, *Scr. Metall.* 9 (11) (1975) 1233–1237.
- [97] A. Barbu, G. Martin, Radiation induced precipitation in nickel silicon solid solutions. ii. dose rate effects, *Scr. Metall.* 11 (9) (1977) 771–775.
- [98] P.D. Edmondson, M.K. Miller, K.A. Powers, R.K. Nanstad, Atom probe tomography characterization of neutron irradiated surveillance samples from the regina reactor pressure vessel, *J. Nucl. Mater.* 470 (2016) 147–154.
- [99] H. Ke, P. Wells, P.D. Edmondson, N. Almirall, L. Barnard, G.R. Odette, D. Morgan, Thermodynamic and kinetic modeling of mn-ni-si precipitates in low-cu reactor pressure vessel steels, *Acta Mater.* 138 (2017) 10–26.
- [100] R. Cauvin, G. Martin, Solid solutions under irradiation. i. a model for radiation-induced metastability, *Phys. Rev. B* 23 (7) (1981) 3322.
- [101] R. Cauvin, G. Martin, Solid solutions under irradiation. ii. radiation-induced precipitation in alzn undersaturated solid solutions, *Phys. Rev. B* 23 (7) (1981) 3333.
- [102] S. Xia, M.C. Gao, T. Yang, P.K. Liaw, Y. Zhang, Phase stability and microstructures of high entropy alloys ion irradiated to high doses, *J. Nucl. Mater.* 480 (2016) 100–108.
- [103] B. Kombaiah, K. Jin, H. Bei, P.D. Edmondson, Y. Zhang, Phase stability of single phase al0.12crnifeco high entropy alloy upon irradiation, *Mater. Des.* 160 (2018) 1208–1216.
- [104] T. Yang, S. Xia, S. Liu, C. Wang, S. Liu, Y. Fang, Y. Zhang, J. Xue, S. Yan, Y. Wang, Precipitation behavior of al x cocrfe ni high entropy alloys under ion irradiation, *Sci. Rep.* 6 (1) (2016) 1–8.
- [105] K. Fujii, K. Fukuya, Effects of radiation on spinodal decomposition of ferrite in duplex stainless steel, *J. Nucl. Mater.* 440 (1–3) (2013) 612–616.
- [106] K. Nakai, C. Kinoshita, Irradiation-induced spinodal decomposition in alloys, *J. Nucl. Mater.* 169 (1989) 116–125.
- [107] T. Koppenaal, W. Yeh, R. Cotterill, Lattice defects in neutron irradiated  $\alpha$  cu solid solution alloys, *Philos. Mag.* 13 (124) (1966) 867–871.
- [108] A. Marwick, Segregation in irradiated alloys: the inverse kirkendall effect and the effect of constitution on void swelling, *J. Phys. F: Met. Phys.* 8 (9) (1978) 1849.
- [109] M. Nastar, F. Soisson, 1.18 radiation-induced segregation, *Compr. Nucl. Mater.* 1 (2012) 471–496.
- [110] A. Marwick, R. Piller, M. Horton, 4 radiation-induced segregation in fe-cr-ni alloys, Dimensional stability and mechanical behaviour of irradiated metals and alloys, Thomas Telford Publishing, 1984, pp. 11–15.
- [111] S. Sun, N. Qiu, K. Zhang, P. He, Y. Ma, F. Gou, Y. Wang, Segregation of al1.5crfe ni high entropy alloys induced by vacancy-type defects, *Scr. Mater.* 161 (2019) 40–43.
- [112] C.M. Barr, J.E. Nathaniel II, K.A. Unocic, J. Liu, Y. Zhang, Y. Wang, M.L. Taheri, Exploring radiation induced segregation mechanisms at grain boundaries in equiatomic cocrfe ni high entropy alloy under heavy ion irradiation, *Scr. Mater.* 156 (2018) 80–84.
- [113] Z. Fan, W. Zhong, K. Jin, H. Bei, Y.N. Osetsky, Y. Zhang, Diffusion-mediated chemical concentration variation and void evolution in ion-irradiated nicofecr high-entropy alloy, *J. Mater. Res.* 36 (1) (2021) 298–310.
- [114] M.-R. He, S. Wang, S. Shi, K. Jin, H. Bei, K. Yasuda, S. Matsumura, K. Higashida, I.M. Robertson, Mechanisms of radiation-induced segregation in crfeconi-based single-phase concentrated solid solution alloys, *Acta Mater.* 126 (2017) 182–193.
- [115] G.S. Was, Fundamentals of Radiation Materials Science: Metals And Alloys, Springer, 2016.
- [116] T. Yang, W. Guo, J.D. Poplawsky, D. Li, L. Wang, Y. Li, W. Hu, M.L. Crespiello, Z. Yan, Y. Zhang, et al., Structural damage and phase stability of al0.3cocrfe ni high entropy alloy under high temperature ion irradiation, *Acta Mater.* 188 (2020) 1–15.
- [117] V.V. Rondinella, T. Wiss, The high burn-up structure in nuclear fuel, *Mater. Today* 13 (12) (2010) 24–32.
- [118] A.R.M. Iasir, N.J. Peters, K.D. Hammond, Estimation of effective thermal conductivity in u-10mo fuels with distributed xenon gas bubbles, *J. Nucl. Mater.* 508 (2018) 159–167.
- [119] V. Zell, H. Schroeder, H. Trinkaus, Helium bubble formation in nickel during hot implantation, *J. Nucl. Mater.* 212 (1994) 358–363.
- [120] L. Yang, H. Ge, J. Zhang, T. Xiong, Q. Jin, Y. Zhou, X. Shao, B. Zhang, Z. Zhu, S. Zheng, et al., High he-ion irradiation resistance of crmfecni high-entropy alloy revealed by comparison study with ni and 304ss, *J. Mater. Sci. Technol.* 35 (3) (2019) 300–305.
- [121] J. Hu, J. Zhang, J. Zhang, H. Xiao, L. Xie, H. Shen, P. Li, G. Sun, X. Zu, Theoretical combined experimental study of unique he behaviors in high-entropy alloys, *Inorg. Chem.* 60 (3) (2021) 1388–1397.
- [122] Z. Zhu, H. Huang, O. Muránsky, J. Liu, Z. Zhu, Y. Huang, On the irradiation tolerance of nano-grained ni-mo-cr alloy: 1 mev he+ irradiation experiment, *J. Nucl. Mater.* 544 (2021) 152694.
- [123] F. Garner, Radiation damage in austenitic steels (ed. rjm konings)/comprehensive nuclear materials. v. 4 (2012).
- [124] B. Raj, M. Vijayalakshmi, Ferritic steels and advanced ferritic-martensitic steels, comprehensive nuclear materials (2012).
- [125] F. Garner, 4.02 radiation damage in austenitic steels, *Compr. Nucl. Mater.* 4 (2012) 33–95.
- [126] A. Etienne, M. Hernández-Mayoral, C. Genevois, B. Radiguet, P. Pareige, Dislocation loop evolution under ion irradiation in austenitic stainless steels, *J. Nucl. Mater.* 400 (1) (2010) 56–63.
- [127] J.-W. Yeh, S.-J. Lin, T.-S. Chin, J.-Y. Gan, S.-K. Chen, T.-T. Shun, C.-H. Tsau, S.-Y. Chou, Formation of simple crystal structures in cu-co-ni-cr-al-fe-ti-v alloys with multiprincipal metallic elements, *Metall. Mater. Trans. A* 35 (8) (2004) 2533–2536.
- [128] Y. Zhou, Y. Zhang, Y. Wang, G. Chen, Solid solution alloys of al co cr fe ni ti x with excellent room-temperature mechanical properties, *Appl. Phys. Lett.* 90 (18) (2007) 181904.
- [129] C.-Y. Hsu, J.-W. Yeh, S.-K. Chen, T.-T. Shun, Wear resistance and high-temperature compression strength of fcc cuconical 0.5 fe alloy with boron addition, *Metall. Mater. Trans. A* 35 (5) (2004) 1465–1469.